1-1-2006

Multi-scale models for wafer surface evolution in chemical mechanical planarization

Xiaoping Wang
Iowa State University

Multi-scale models for wafer surface evolution in chemical mechanical planarization

by

Xiaoping Wang

A thesis submitted to the graduate faculty

in partial fulfillment of the requirements for the degree of

MASTER OF SCIENCE

Major: Mechanical Engineering

Program of Study Committee:
Abhijit Chandra, Co-major Professor
Ashraf Bastawros, Co-major Professor
Thomas J. Rudolphi

Iowa State University

Ames, Iowa

2006

Graduate College
Iowa State University

This is to certify that the master's thesis of

Xiaoping Wang

has met the thesis requirements of Iowa State University

Signatures have been redacted for privacy

TABLE OF CONTENTS

LIST OF FIGURES

LIST OF TABLES

ACKNOWLEDGEMENTS

I would like to express my gratitude and appreciation to my advisors, Dr. Abhijit Chandra and Dr. Ashraf Bastawros. I am truly thankful for their valuable guidance and support. I am particularly thankful to Dr. Chandra for his patience and encouragement through out the research and the writing of thesis. I would also like to thank Dr. Thomas J. Rudolphi who served as my POS committee member and helped a lot on my study.

Dr. Sutee Eamkajomsiri, Karra Pavan Kumar, Bun Hiong Chua, and Ruqin Zhang are gratefully acknowledged for their contribution to this research by their valuable dissuasions and friendship.

I would like to thank my husband, Chengzhi Tang. He was always with me during these years. The work would not have been possible without him. I would like to thank my parents for their love and support during my life.

ABSTRACT

As device size decreases and circuit density increases, planarization technology becomes more and more important in semiconductor fabrication. Chemical mechanical planarization (CMP) was introduced into semiconductor fabrication process during early 1990s and has emerged as a new promising technique for its capability to achieve better local and global planarization of wafer surface. Although CMP has been widely used in many areas, such as inter-level dielectric, copper damascene, and shallow trench isolation, etc., it is still far from fully understood. To optimize the process, many issues still need further investigations. One of the most important and powerful approaches is CMP modeling, which is able to combine the fundamental understandings of CMP process and provide a broad picture of how all the involved components interact. With CMP modeling, optimized polishing control schemes and process improvement directions can be obtained with much less cost than experimentation. It is also a promising tool for new process development.

CMP process is sensitive to the pattern density variation across a chip. The material removal rates are different for the regions with different pattern density. For a region with a higher pattern density, the material removal rate on up area is faster. For a region with a lower pattern density, the material removal rate on up area is slower. Therefore, CMP obtains the local planarization but generates global steps. Two models, referred as Models I and II, are developed to investigate the pattern density effect on the post-CMP wafer surface profile.

Model I assumes that the pad asperities contact with the wafer surface directly without considering the effects of slurry particles. In developing this model, at first, the pressure distribution between a rough pad and a patterned wafer is evaluated based on the work of Greenwood and Williamson (1966); then, approaches are proposed to re-distribute the pressure due to pad bending to account for the effects of surrounding topography. The modified pressure is then utilized in Archard's law (1953) to predict the local material

removal rate and associated wafer surface evolution. This model has been verified against the experimental observations of Ouma et al. (2002). A parametric study is conducted using this model to investigate the effects of pad roughness, bending ability, and influence length (which is defined the range of area over which the surrounding features affect the material removal rate at a given location). CMP designs for effective planarization are discussed.

Model II extends Model I to account for the effects of abrasive particles. The wafer material removal is assumed to be primarily due to the abrasive wearing of slurry particles. Different from previous models based on the slurry particles wear mechanism, Model II evaluates the MRR distribution on the wafer surface and the wafer profile evolution. Modeling is focused on a small region on the wafer surface. The contact pressure at this region is evaluated by Model I first. Then the material removed by a single active particle sliding over this region is estimated. After estimating the number of active particles sliding over this region during a time step, the total material removed from this region and the mean material removal rate can be calculated. By doing this across the whole wafer surface, the wafer profile evolution is obtained.

Chapter 1: Introduction

With the shrinkage of device dimension and the increase of circuit density, planarization technology becomes more and more important in semiconductor fabrication. Chemical mechanical planarization (CMP) was introduced into processing during early 1990s and has emerged as a new promising technique for its capability to achieve better local and global planarization of wafer surfaces (Steigerwald et al., 1997) and its ability to planarize over longer length scales than traditional planarization techniques.

1.1 CMP Process

Figure 1.1 schematically shows a conceptual diagram of CMP apparatus. The wafer is mounted on a rotating carrier and is brought into contact with a polishing pad mounted on a rotating platen. During a CMP process, slurry is flowed onto the interface between wafer and pad. A combination of the mechanical down force applied by wafer carrier as well as the chemical action of the slurry is used to polish the wafer surface. A pad conditioner is used to recover the pad topography.

Polishing pad, wafer carrier, slurry and pad conditioner are the four major components in a CMP process. A polishing pad is made up from polyurethane whose properties can be readily and precisely controlled. Its surface topography and mechanical properties (i.e. Young's modulus, Poisson ratio, compressibility and visco-elastic properties) have significant influences on the quality and efficacy of a CMP process. A brief discussion of pad topography and its effects on CMP process will be given in Chapter 2.

Slurry consists of nano-scale abrasive particles and chemical solution. Different types of slurries may behave differently according to their abrasive particles materials and the solution chemical properties. The chemical solution reacts with the wafer surface to weaken the surface material to make it easier to be removed. The abrasive particles act as cutting

tools and involve in the repeated plowing action leading to material removal of the soften wafer surface (Fu, 2002). In general, abrasives are inorganic oxides. The most commonly used abrasives in CMP slurries are silica (SiO_2) and alumina (Al_2O_3). In addition, the particles size and its distribution significantly affected the material removal rate in CMP (Luo et al., 2001, 2003; Zhao et al., 2002; Wang et al., 2005; Zeng et al., 2005).

A wafer carrier transmits the down force to the wafer surface and ensures that the wafer remains in place while it is being polished. It also defines the pressure distribution across the wafer surface during a CMP process. The present state of art carriers provides an ability to adjust the pressure in different zones across the wafer surface, and thus improve the quality of polished surface. The typical wafer carrier design can be found in Oliver (2004).

A pad conditioner is a diamond-impregnated disk, which abrades the pad surface and restores the pad roughness during CMP, and thus stabilizes the removal rate. Without conditioning, glazed areas due to the cold flow of pad material (Bajaj et al., 1994) will be generated on the pad surface, which will reduce the pad porosity and surface roughness. Consequently, the material removal rate will drop rapidly and wafer surface planarity will become unacceptable.

1.2 Applications of CMP

Applications of Chemical mechanical planarization have been widely seen in sub-micron integrated circuit (IC) fabrication in the last fifteen years (Luo and Dornfeld, 2004). Three major application areas are inter-level dielectric (ILD), copper damascene process, and shallow trench isolation (STI).

An interlevel dielectric, consisting of sputtered SiO_2 or a plastic-like material called polyimide, is deposited onto the patterned metal layer to perform as an insulator. With the increase in device density, multilevel metal interconnect is strongly required in semiconductor fabrication. A multilayer ILD is also needed to fabricate such multilevel metal system. During the fabrication, the topology of the earlier layers is critical for the later layer

process. CMP was used to fabricate multilevel metallization due to its ability to achieve highly planar layers. Figure 1.2 schematically shows the process flow of a one-level ILD. This process includes: i) patterning the metal layer using subtractive etching technique, ii) depositing dielectric material on the top of metal, and then iii) planarizing dielectric layer with a CMP process. Compared to conventional methods such as spin-on-glass and sacrificial-resist-etch back (Wolf, 1990), which only provide a local planarization over several microns, CMP can planarize a distance up to several millimeters. Without CMP, the non-planarization of ILD layers accumulates from lower levels to higher levels and causes three main problems: i) the inaccuracy of following pattern occurs due to the limitation of lithography depth of focus, ii) the step-coverage of metal line causes open circuits in the thin metal film, and iii) the remaining metal stringers will result in short circuits between adjacent lines (Ouma, 1998).

Propagation delay associated with interconnects is an essential part to define the performance of a integrate circuit. It can be decreased by reducing either the resistance or capacitance of interconnects. Since copper has a lower resistivity compared with the conventional material, aluminum (Al), it is being used as the interconnect material in IC manufacturing. The lower resistivity of copper, combined with the introduction of low-dielectrics, reduces time delays and power consumption (Singer, 1998). Since copper cannot be easily etched like Al, CMP is currently the only method that enables the use of copper damascene process. Figure 1.3 shows the process flow of copper damascene. The designed interconnect pattern is first etched into a planar dielectric surface using a standard photolithography technique. Following that is a barrier layer deposition process. Then the entire surface is electroplated, filling the interconnect regions as well as covering the rest of the surface with copper. In the end the extra copper is polished and planarized using a CMP process.

STI is another application of CMP and has become a key technology for device isolation (Patrick, 1991and Lee, 2001). The process flow of STI is given in Figure 1.4. Firstly,

Nitride film is deposited onto a planarized silicon substrate. Shallow trenches are then etched onto the substrate and silicon oxides are deposited into these trenches. After that the silicon oxide layer is planarized with a CMP process until the nitride film is exposed. Lastly the nitride is removed. The details of STI structures fabrication have been discussed in Jeong et al. (2003). STI is able to separate elements within a much narrower area, and shows much better performance than the conventional local oxidation of silicon (LOCOS) method, which causes bird's beak structures (Jaeger, 2002).

Although CMP has wide applications and advantages in IC fabrication, many issues still need to be investigated and optimized. They are related to four length scales, namely, particle, feature, die and wafer scales (shown in Figure1.5). The particle scale is smaller than the feature scale. At the particle scale, material removal rate and surface quality are the two most important issues to investigate. It is critical to understand the interactions of the abrasive particles/the pad topography/wafer surface, and the material removal mechanism. At the feature scale, major concerns include the step height reduction, dishing and erosion. At the die scale, CMP is sensitive to different pattern densities, which results in with-in die non-uniformity (WIDNU). At the wafer scale, the major interest is with-in wafer non-uniformity (WIWNU), which is mainly due to the non-uniform distribution of pressure and velocity across the wafer. CMP modeling provides insights into the fundamental processes that can control polishing, supplies directions for CMP optimization, and thus improve product yields.

1.3 Review of CMP Models

A CMP process is very complicated with many variables involved (Luo, 2004). The influencing factors include tool process parameters (i.e. pressure or force applied to the wafer and pad, wafer-pad relative velocity, etc.), wafer variables (i.e. wafer materials and surface geometry), slurry variables (i.e. chemical properties, particle size and its distribution, etc.), and pad variables (i.e. pad materials and topography, etc.). Many experimental investigations

have been done to understand the CMP process and various kinds of models have been developed to simulate the different aspects of CMP. In this section, a brief review of CMP models in provided. The models will be reviewed by particle scale, feature-die scale, and wafer scale. Some concepts used in the models are shown in Figure 1.6.

Particle Scale

Material removal rate investigation is a main focus at particle scale. The most basic material removal rate equation is the so-called Preston's equation (1927), which was initially introduced for glass polishing. It assumes that the material removal rate (MRR) depends linearly on the pressure and velocity by

$$MRR = \frac{dH}{dt} = K_p PV \tag{1.1}$$

where K_p is the Preston coefficient. P is the local pressure on wafer; and V is the relative velocity at a point on the wafer surface related to the pad. Although this equation has been widely used in CMP process modeling, it does not show the effects of various process variables on MRR. Recent experiment results have demonstrated that pad properties and abrasive particles size and concentration have significant effects on MRR variation. Hence, further development of the modeling framework is needed to address the various aspects of CMP process and the influences of important CMP process parameters.

Cook (1990) developed a model to address the physical meaning of CMP process by extending Brown's model (1981) of the metal polishing to the silicon polishing. It was assumed that the slurry particles undergo the polishing. The interaction between the abrasive particles and the wafer surface was modeled as Hertzian elastic penetration of a spherical particle under uniform pressure P into the wafer surface. The polishing rate was then given by

$$MRR = \frac{1}{2E_w} PV \tag{1.2}$$

where E_w is the Young's modulus of the wafer material.

Zhao and Shi (1998, 1999) proposed a model based on the assumption of elastic contact between the wafer/pad/abrasive particles. In their model, they studied the fundamental mechanism for the pressure dependence of polishing rate in CMP process with a soft pad. The nonlinear pressure dependence of material removal rate was shown due to the nonlinear pressure dependence of contact area between the wafer and pad. The resulting removal rate was given by:

$$MRR = K_p P^{\frac{2}{3}} V \tag{1.3}$$

This model assumed that the wafer was polished due to the abrasive particles indentation. Since the MRR is linearly related to the number of abrasives involved in material removal and the number of abrasives depends on the contact area between the wafer and pad (which is nonlinearly depends on the pressure), the MRR was nonlinearly dependent on the pressure. A "threshold pressure" concept was also introduced by Zhao and Shi (1998, 1999) arguing that material removal took place only when this pressure was exceeded.

Luo et al. (2001, 2003) investigated the interactions between the wafer, pad, and abrasive particles. A comprehensive model was proposed to describe material removal rate. This model assumed of plastic contact over wafer-abrasive and pad-abrasive interfaces, the normal distribution of abrasive particle size and periodic roughness of pad surface. An approach was proposed to estimate the number of particles which contribute the material removal. The model integrated the process parameters (i.e. pressure and velocity) and other important parameters, including the wafer hardness, pad hardness, pad roughness, abrasive size into a single formulation to predict the material removal rate. It was found that the material removal rate nonlinearly depends on the down pressure and is related to the mean particles size, the particle size distribution, and the pad deformation.

Zhao et al. (2002) proposed a micro-contact and wear model, which is similar with Luo's model (2001, 2003). However, they assumed that the pad asperity height is of a random distribution and the particle size is uniformly distributed, and the estimation of the

active particle number is much different. The two different approaches will be described in Chapter 3.

Wang et al. (2005) proposed a model by combining the elements of models presented by Luo et al. (2001, 2003) and Zhao et al. (2002) with the time decay MRR models in Wang et al. (2005). This model is able to capture the effects of particle size, pad roughness, as well as the time varying of the MRR due to pad surface topography evolution.

Feature-Die Scale

At the feature and die scales, significant research work have been devoted to model the with-in die non-uniformity (Ouma et al., 1998), dishing and erosion (Fu et al., 2003; Vlassak, 2004). A number of models have been presented to predict the wafer profile evolution during the polishing process to prevent these problems (Warnock, 1991; Chekina et al., 1998; Ouma et al., 1998; Vlassak, 2004).

Warnock (1991) proposed a phenomenological model that allows quantitative prediction of wafer topography. In this model, the removal rate at a given point was assumed to be affected by the surrounding features. Higher surrounding features decrease the removal rate, while lower surrounding features enhance it. Three adjustable parameters were used to describe the pad deformation, the pad roughness and the relative velocity respectively. The model accurately predicted the experiment data. However, three parameters have no direct physical implication.

A contact wear model by Chekina et al. (1998) was used to predict wafer topography evolution at feature scale. The pressure distribution along wafer surface was studied based on contact mechanics, taking account of the pad elastic deformation. Vlassak (2004) developed another contact mechanics based model, which takes into account both the roughness and elastic deformation of the polishing pad in computing the pressure distribution. Roughness of the pad was considered by the contact model of Greenwood and Williamson (1966). This model is able to evaluate the evolution of the wafer profile during the CMP process. It depends on an iterative solution procedure, where two equations describing the pressure

distribution between the polishing pad and wafer, and the pad deformation need to be iteratively solved. This procedure requires a significant amount of computation to reach the convergence.

Ouma et al. (2002) developed a model to predict the wafer surface profile across a chip. A concept "effective pattern density (EPD)" was introduced in this model. The removal rate was assumed to depend on the EPD and the blanket wafer polish rate (BWPR). The EPD was calculated with a proposed procedure based on the pad deformation, while the BWPR was determined by experiments. In this model, it was assumed that the down area was not polished until the up area was worn out completely.

Fu et al. (2003) presented an analytical dishing and step height reduction model for CMP. They assumed i) the pad contacts with wafer at any point of the interference; ii) the higher area will release the pressure on the adjacent lower area; iii) the force redistribution due to pad bending is proportional to dishing/step height. This model gives analytical prediction for step height reduction and dishing. The bending factor α that the authors introduced in their model to describe the force redistribution due to pad bending will be given a brief description later and used in this thesis with some modifications.

Wafer Scale

WIWNU at the wafer scale due to the MRR variation across the wafer significantly affects the planarization quality of the wafer. Various proposed models suggest that the MRR is strongly influenced by the interface pressure distribution and the relative velocity. Modeling of the interface pressure and relative velocity facilitates the determination of optimal polishing conditions for obtaining a better surface planarity.

Taking into account the bending of the polishing pad, Sivaram et al. (1992) investigated wafer scale MRR variations by modifying Preston's equation via varying the contact pressure according to the deflection profile. Runnels and Renteln (1993) proposed a model, which focuses on the modeling of the pad deflection at the wafer edge and the resulting stress distribution. Wang et al. (1997) investigated the effects of various process

parameters on the degree of wafer scale non-uniformity. They developed a finite element model to evaluate the pressure distribution by assuming direct wafer-pad contact. The edge effect, i.e., the large material removal rate at the wafer edge, was well explained by the pressure singularity at the edge. Sundararajan et al. (1999) and Thakurta et al. (2000, 2002) developed a sophisticated wafer-scale model that accounts for slurry hydrodynamics and mass transport. The lubrication theory was used to calculate the slurry film thickness for given operating parameters. The model took into account pad compressibility, pad porosity, and the mode of slurry delivery to the polishing pad. Tichy et al. (1999) developed another model to treat the CMP process as a contact problem between a wafer and a rough pad lubricated by slurry. The slurry film thickness was assumed to be equal to the height of the pad asperity. Reynolds equation was utilized to calculate the interfacial pressure. Shan et al. (2000) concluded that the generation of WIWNU was due to a non-uniform subambient fluid pressure between the wafer and pad. In their work, an analytical model was proposed to predict the magnitude and distribution of the interfacial fluid pressure. Fu and Chandra (2001, 2002) presented an analytical solution to evaluate the interface pressure distribution across the wafer based on the assumption that a pad is an elastic / visco-elastic half-space. This model claimed that the interface pressure exhibits significant variation depending on the wafer curvature and polishing conditions.

The relative velocity between the wafer and pad is another important factor for WIWUN at the wafer scale. Olive (2004) provided a detail analysis of kinetics/velocity for various CMP systems.

1.4 Thesis Goals

The goal of this thesis is to understand the chemical mechanical planarization process, investigate the material removal mechanisms at die-feature scale, study the pattern density effect on the post-CMP wafer surface, model the wafer surface profile and provide insights to guide the CMP process designs for effective planarization. In order to reliably predict the

post-CMP wafer profile, the accurate evaluation of the local contact pressure which determines the MRR is a critical factor. It is investigated by Model I based on the work of Greenwood and Williamson (1966). Two parameters (bending factor and influence length) are identified to take account for the surrounding topography effect on the pressure of a given point. The slurry particle size and its distribution have important effects on the MRR in CMP (Luo et al., 2001, 2003; Zhao et al., 2002; Wang et al., 2005). By extending Model I, Model II is proposed to consider the slurry particles effects.

1.5 Thesis Outline

In chapter 2, Model I is proposed to describe the evolution of the patterned wafer surface at the die-feature scale during CMP process. The model assumes that wafer contact with the pad asperity directly ignoring the effect of slurry particles. The Greenwood and Williamson model is applied to evaluate the contact pressure on the interface between a patterned wafer and a rough pad. The effective local contact pressure at any point on the wafer surface is obtained using two proposed approaches to account for the effect of surrounding wafer topography. It is then utilized in Archard's law (1953) to predict the local material removal rate and associated wafer surface evolution.

In chapter 3, Model II is developed to investigate the wafer surface evolution based on the abrasive particles wear mechanism. Different from the particle abrasion based models reviewed in section 1.3, Model II attempts to investigate the MRR at any location. A small region on the wafer surface is then focused. In order to evaluate the MRR at the focused a region, three variables needed to determine include: i) the contact pressure applied at this region, ii) the number of the active particles which slide over this region during a time step, and iii) the material removed by a single active particle under the applied pressure when it plows across the focused region on the wafer surface. When all the three variables are obtained, the Local MRR and the wafer surface evolution can be obtained. The effect of particle size distribution based on Model II is studied in this chapter.

In Chapter 4, conclusions as well as suggestions for future work are given.

Figure 1.1: The schematic illustration of CMP machine.

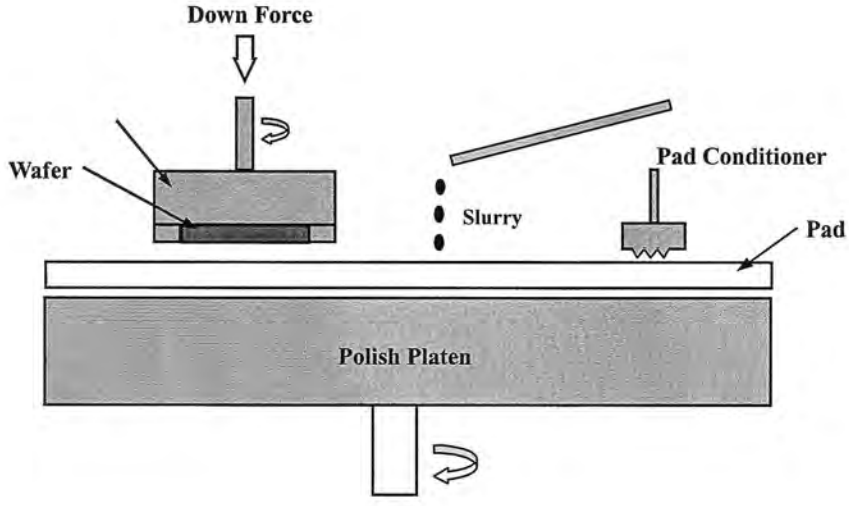

Figure 1.2: The schematic of ILD process.

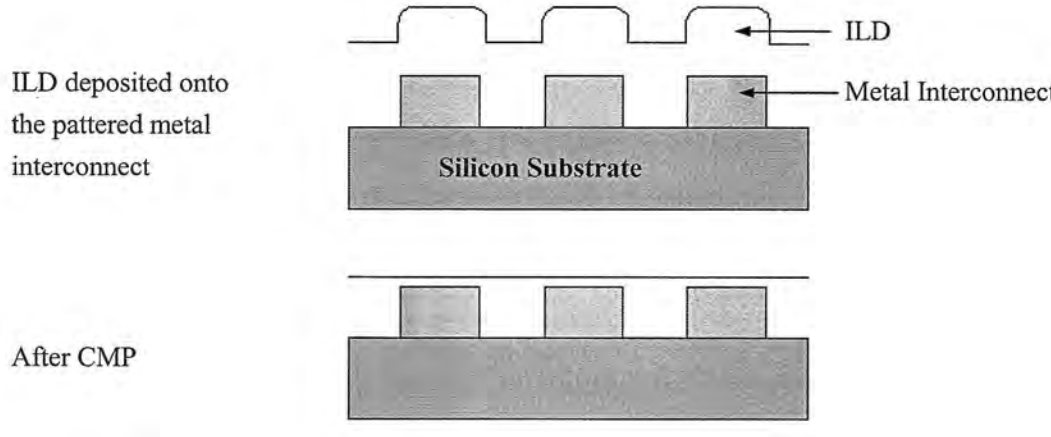

Figure 1.3: The schematic of copper damascene process.

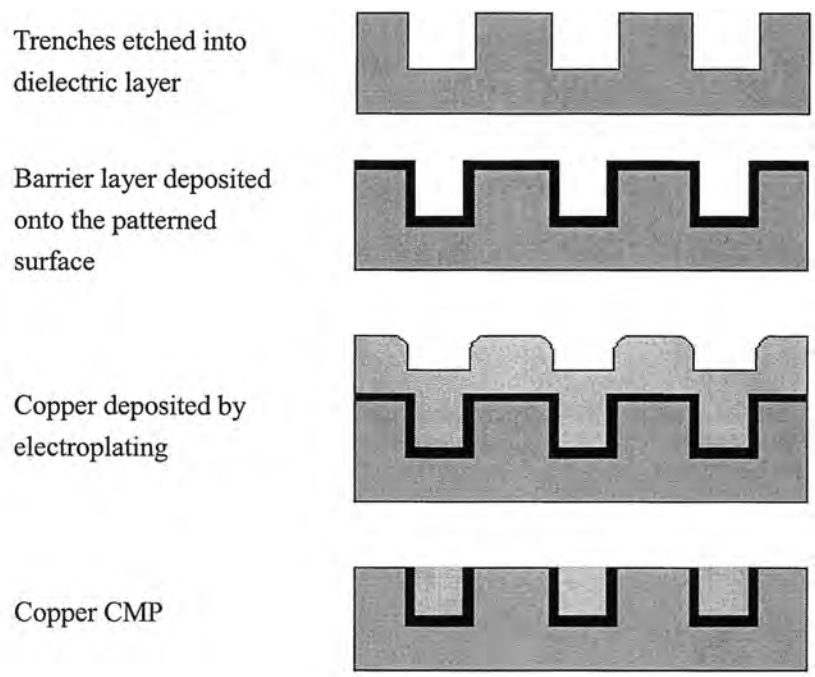

Figure 1.4: The schematic of copper STI process.

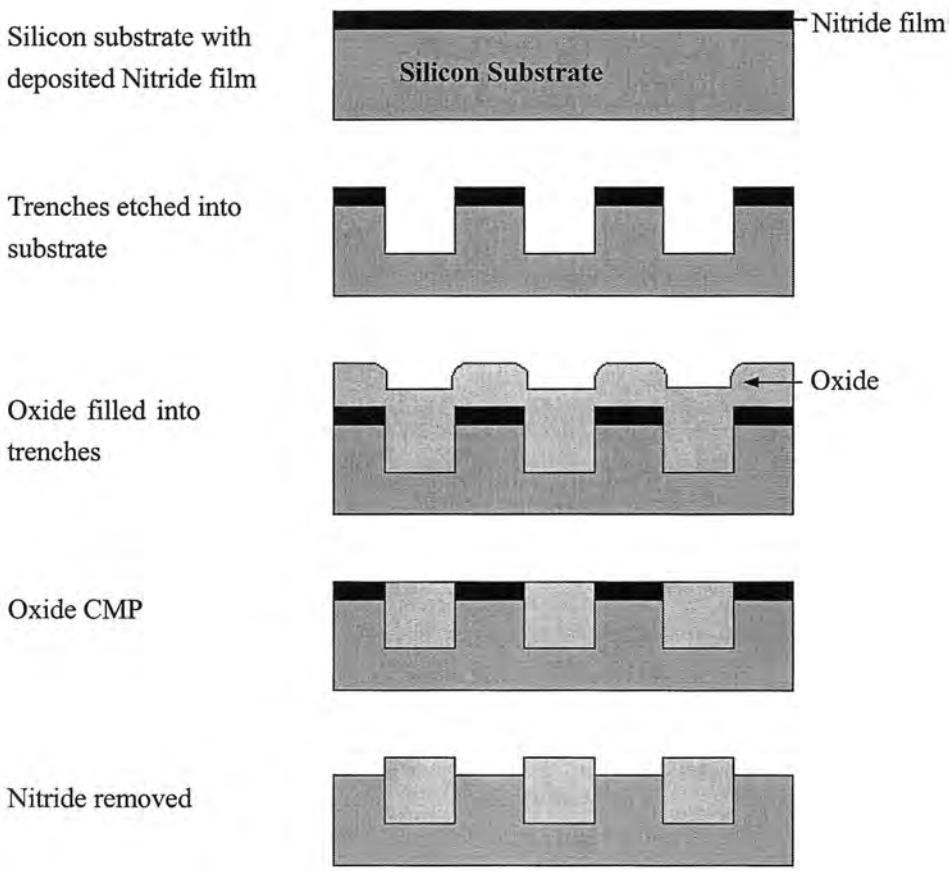

Figure 1.5: The scales map in CMP.

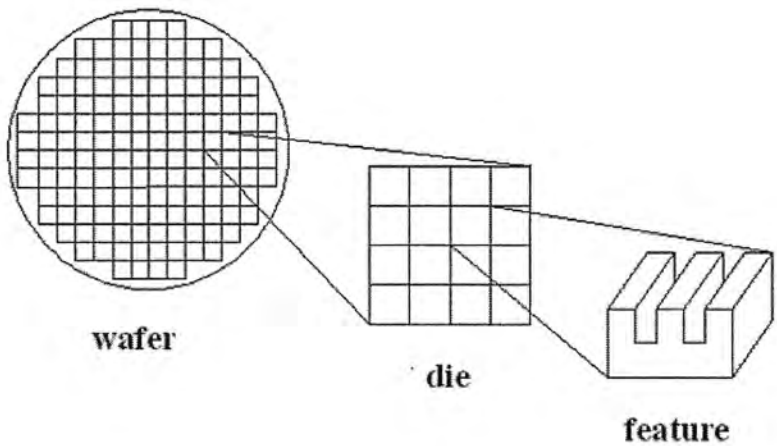

Figure 1.6: The concepts in CMP modeling.

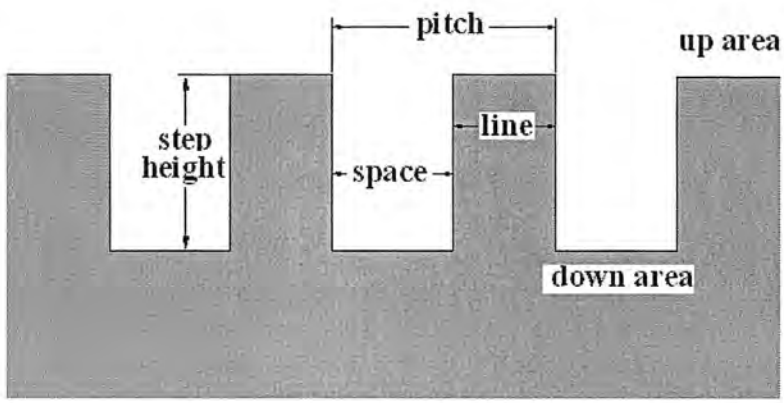

Chapter 2: Pattern Density Effect on Wafer Surface Evolution in Chemical Mechanical Planarization

Compared with traditional planarization techniques, CMP achieves better local and global planarization of wafer surfaces. But CMP process is sensitive to the pattern density variation across the chip, which leads to large variation in global thickness across the die. Therefore, CMP obtains the local planarization but generates global steps as illustrated in Figure 2.1. The initial difference in layout pattern density creates a global step height between these two regions due to the difference in removal rates before the local patterns are planarized (Ouma et al., 1998). The global thickness variation has a serious impact on subsequent process steps such as lithography and etching. It also impacts circuit performance: long-range clock wires passing through regions of different thickness result in different capacitances and may result in clock skew (Stine et al., 1997). Thus, the wafer topography modeling at die scale plays an important role in optimizing the CMP process and layout density design.

In this chapter, a new multi-scale model is presented to describe the evolution of the wafer surface during a CMP process. The model assumes direct contact between a patterned wafer and a rough polishing pad. It ignores the effects of abrasive particles at the feature scale. However, these effects may be introduced at the particle (nano) scale (Wang et al., 2005). The pad asperities are assumed with random height distribution, spherical tips, and periodical spacing across the pad surface. A brief description of pad topography characterization is provided in section 2.1. In section 2.2, a solid-solid contact model based on the work of Greenwood and Williamson (1966) is utilized to determine the mean pressure at any point on the patterned wafer surface. Then two approaches are proposed to re-distribute the pressure due to the effect of the surrounding topography at a given location. The modified pressure is then used to determine the local material removal rate (MRR) using

Archard's wear law (1953). The model is validated in section 2.3 at both die scale and feature scale against the experimental observations of Ouma et al. (2002). In section 2.4, a parametric study is conducted to investigate the effects of polishing pad properties on the post-CMP wafer topography. Insights gathered from this investigation are discussed in section 2.5

2.1 Pad Surface Characterization

The topography of polishing pads plays a significant role in CMP processes. Some characterization of the polishing pad is given based on a representative IC 1000 pad (Bastawros et al., 2002; Borucki, 2002; Guo et al., 2004; and Wang et al., 2005). The pad surface has numerous pores with an average pore diameter of 30~50 μm. These pores typically occupy about 35% of the volume of the material and are separated by polyurethane membranes, which form asperities/roughness on the polishing pad. During a polishing process, it is these asperities that actually contact with the wafer surface. The real contact area is usually very small and is about 1% or less of the nominal contact area between the wafer and pad (Shan, 2000). The real contact pressure is then much higher than the nominal pressure and directly affects the material removal rate in CMP. The pad topography can be characterized by the probability density function (PDF) of pad asperities heights. Yu (1993) suggested a Gaussian distribution to describe the height distribution of the pad asperity. Borucki (2002) and Wang et al. (2005) used a Pearson IV PDF to model the rough surface of pad. Vlassak (2004) applied an exponential distribution to reduce the computation in the model. The pad asperity height PDF can be determined by statistical parameters such as mean, standard deviation, skew and kurtosis. Table 2.1 presents the values of these statistical parameters that will be used in the simulation (Stein, 1996; Wang et al., 2005). Those values determine that the pad asperity height is distributed as a Pearson IV PDF (Johnson, 1970). The asperity tip radius which is assumed to be constant and the asperity density used in the model are also given in Table 2.1.

2.2 Model Development

2.2.1 Contact model description

Greenwood and Williamson (1966) developed a model (Figure 2.2) for contact between a smooth flat surface and a rough surface using Hertzian contact theory (Johnson, 1985). Adapting this model to the CMP process simulation, the wafer surface is assumed to be smooth and flat on the global scale, while the pad surface is assumed to be rough and contains asperities with a given height PDF $\phi(Z_p)$ relative to the mean plane of surface. The asperities assume to be uniformly spaced across the pad surface with an area density η_s. All asperities are assumed have spherical tips, each with an identical radius R_p.

The separation distance d in Figure 2.2 is defined as the distance between mean plane of the pad and the smooth wafer surface. For an asperity with height Z_p larger than d, it will carry a load (according to Hertzian contact theory)

$$L = \frac{4}{3} E^* R^{*\frac{1}{2}} (Z_p - d)^{\frac{3}{2}} \tag{2.1}$$

The contact area between the asperity and the wafer is

$$A_c = \pi R^* (Z_p - d) \tag{2.2}$$

The total load L_{total} and real contact area A_{re} by all pad asperities are giving by the mean load/mean contact area for one single asperity multiplied by the total number of the pad asperities:

$$L_{total}(d) = A_o \eta_s \int_{Z_p - d > 0} \frac{4}{3} E^* R^{*\frac{1}{2}} (Z_p - d)^{\frac{3}{2}} \phi(Z_p) dZ_p \tag{2.3}$$

$$A_{re}(d) = A_o \eta_s \int_{Z_p - d > 0} \pi R^* (Z_p - d) dZ_p \tag{2.4}$$

Where R^* is the equivalent radius given by

$$\frac{1}{R^*} = \frac{1}{R_p} + \frac{1}{R_w} \tag{2.5}$$

R_p and R_w are the asperity radius of pad and wafer respectively. The wafer surface is assumed has very larger radius compared with the pad asperity. Thus $R^* \approx R_p$. E^* is the equivalent modulus. It is given by

$$\frac{1}{E^*} = \frac{1-\nu_w^2}{E_w} + \frac{1-\nu_p^2}{E_p} \tag{2.6}$$

E_w and E_p are the Young's modulus of wafer and pad respectively; ν_w and ν_p are Poisson's ratio of wafer and pad respectively. Usually $E^* \approx E_p/(1-\nu_p^2)$ since E_w is much larger than E_p.

According to Greenwood and Williamson (1966) model, the load balancing equation between the nominal pressure $\overline{P}$ applied on the wafer surface and the separation distance d is given by

$$\overline{P} = \frac{L_{total}(d)}{A_o} = \frac{4\eta_s E^* R^{*\frac{1}{2}}}{3} \int_{Z_p - d>0} (Z_p - d)^{\frac{3}{2}} \phi(Z_p) dZ_p \tag{2.7}$$

Then the ratio A_f of the real contact area A_{re} to the nominal area A_o is

$$A_f = \frac{A_{re}(d)}{A_o} = \pi\eta_s R^* \int_{Z_p - d>0} (Z_p - d)\phi(Z_p) dZ_p \tag{2.8}$$

Following Archard's law (1953), it was assumed that the material removal rate (MRR) is proportional to the average real contact pressure.

$$P_{re} = \frac{L_{total}(d)}{A_{re}(d)} = \frac{\overline{P}A_o}{A_{re}(d)} = \frac{\overline{P}}{A_f} \tag{2.9a}$$

$$\overline{MRR} = C_w P_{re} \tag{2.9b}$$

Where C_w is a coefficient of proportionality. It is proportional to the relative velocity between the wafer and pad and related to wafer and pad material properties. The above equation is a form of Archard's law (1953). It is similar to the Preston's equation (Preston, 1927).

The model described above assumed that the wafer surface is smooth. However, in most situations, the wafer has a patterned surface, instead of a smooth surface. Figure 2.3 shows the schematic of the CMP model described in this chapter. The pad is full of asperities which has the properties described in section 2.1. The wafer surface has different heights Z_w referred to its mean plane. Z_w is assumed to have a distribution $\psi(Z_w)$ which is independent with $\phi(Z_p)$. Then it follows that balancing equation (7) can be modified by considering an equivalent joint distribution for $(Z_p + Z_w)$ as

$$\overline{P} = \frac{4\eta_s E^* R^{*\frac{1}{2}}}{3} \int_{Z_p+Z_w-d>0} (Z_p + Z_w - d)^{\frac{3}{2}} \phi(Z_p)\psi(Z_w) dZ_p dZ_w \tag{2.10}$$

From Eq. (2.10), the load-balancing separation d can be solved providing $\overline{P}$, $\phi(Z_p)$, $\psi(Z_w)$ and η_s, E^*, R^* are given. Due to the fact that the wafer surface height is much smaller compared with the height of pad asperity, the effect of the wafer surface height on the separation distance d can be neglected. Then, Eq. (2.10) can be simplified as Eq. (2.7).

After knowing the load-balancing separation distance d, the mean pressure $\tilde{P}(x)$ at any point on wafer during time step Δt can be calculated as following.

During the time step Δt, many pad asperities contact with the wafer at point x_i one after another assuming Δt is sufficiently large that these contacting pad asperities follow the height distribution $\phi(Z_p)$. d is assumed to be constant during Δt. If the effect of surrounding wafer topography is not considered, then the mean contact pressure at point x_i during Δt is equal to the real contact pressure between a rough pad and a local smooth wafer with a separation distance $\tilde{d} = d - Z_w(x_i)$:

$$\tilde{P}(x_i) = \frac{L_{total}(\tilde{d})}{A_{re}(\tilde{d})} \tag{2.11}$$

2.2.2 Effect of surrounding topography

Warnock (1991) points out that depending on the pad flexibility, polishing rate at any given point is affected by its surrounding topography. Fu et al. (2003) proposed an approach for pressure redistribution to consider the surrounding topography effect. A brief description of their approach is given through Figure 2.4 (a). h is the step height between the up area and the down area. They assumed that the pad contacts with the wafer completely and deforms like a set of linear elastic springs. The pressures for up area and down area were $\widetilde{P}_{up}$ and $\widetilde{P}_{down}$ respectively without considering the effects of surrounding features. Due to the pad bending, there is force redistribution between the up area and the down area. The force change ΔF is assumed to be proportional to height difference

$$\Delta F = \alpha \cdot h \tag{2.12}$$

where α is defined as the bending factor and the unit is N/m^2. ΔF is a line load by assuming the uniform state along the direction into the page. Then the pressures $\widetilde{P}_{down}$ and $\widetilde{P}_{up}$ were changed to

$$P^*_{up} = \widetilde{P}_{up} + \frac{\Delta F}{(b-a)} \tag{2.13}$$

$$P^*_{down} = \widetilde{P}_{down} - \frac{\Delta F}{a} \tag{2.14}$$

The pressure on the up area and down area were changed evenly neglecting the fact that the point on up area nearer to the down area should carry more load and the point on down area nearer to the up area should be released more load (Choi et al., 2006). In other words, the effect of surrounding topography on a given point pressure was the same if the surrounding points had the same height difference with the given point, regardless of the effect of the distance between the given point and the surrounding points. In fact, for the surrounding points with same height difference, the point with a smaller distance from a given point will make a larger influence. An appropriate weight function may be introduced to address this influence of proximity.

The model of Fu and Chandra (2003) assumes that the pad contacts with the wafer surface completely. This is true when the step height between the up area and the down area is small enough. However, at the beginning of the CMP process, the pad may not contact completely with the wafer. Accordingly, two approaches are used in the present work to re-distribute the pressure due to the pad bending.

The first approach is used when the step height h is larger than a critical contact height (H) and the pad does not contact with the down area of the wafer. This contact height (H) depends on the width of the down area (Smith et al., 1999) for specified pressure. When the down area is wider, the contact height (H) is larger.

The second approach is a modified version of Fu and Chandra (2003). It is used when the pad contacts with the wafer completely, i.e. the step height h is smaller than H. The case where the pad contacts with the down area partially is not considered here for simplicity.

A combination of these two approaches is used in the current work to consider the influence of the surrounding topography.

1) The pad does not contact with the down area of wafer due to the surrounding up area as in Figure 2.4 (b). This is the case if the step height h is large and the space width a is small such that the high area relieves the load on down area completely. Pressure redistribution is done in the following way. The load carried by down area is assumed to be supported evenly by the up area. After calculating the average pressure $\widetilde{P}_{down}$ without considering the surrounding point effect, we simply release the load carried by down area a and completely transfer it to the surrounding up area (b-a) by

$$\Delta P = \frac{\widetilde{P}_{down} \cdot a}{(b-a)} \tag{2.15}$$

Then

$$P^*_{down} = 0 \tag{2.16a}$$

$$P_{up}^{*} = \widetilde{P}_{up} + \Delta P \tag{2.16b}$$

Where $\widetilde{P}_{down}$ and $\widetilde{P}_{up}$ are the local contact pressure calculated by Eq. (2.11) without considering the effect of the surrounding topography.

2) As the step height h decreases, the pad contacts with the down area of the wafer completely as in Figure 2.4(a). Then the pressure redistribution method of Fu and Chandra (2003) is modified to obtain the pressure redistribution. The pressure change of a given point due to a neighboring point with the height difference h is given by

$$\Delta P = \widehat{\alpha} \cdot h \tag{2.17}$$

The definition of $\widehat{\alpha}$ here is the pressure change of a given point by a neighboring point with a unit height difference. The unit of $\widehat{\alpha}$ is N/m^3. It is different from α defined in Fu et al. (2003) for plane strain condition, but represents a similar idea. So we still call it the pad bending factor and denote it with α later. For a pad that bends easily, the bending factor is typically smaller since the higher point will relieve less pressure off the lower point.

In this model, it is assumed that the pressure at any point on the wafer is affected by the surrounding topography within an influence length l over which the pad bends. So, the pressure could be changed by

$$\Delta P(x_i) = \int_{x_i - l/2}^{x_i + l/2} w(x_i - x) \cdot \alpha \cdot \left[Z_w(x_i) - Z_w(x) \right] \mathrm{d}x \tag{2.18}$$

$$P^{*}(x_i) = \widetilde{P}(x_i) + \Delta P(x_i) \tag{2.19}$$

Where $Z_w(x_i)$-$Z_w(x)$ is the height difference, and x_i-x is the distance between two points (within the influence zone) on the wafer. $\widetilde{P}(x_i)$ is the pressure calculated using Eq. (2.11). $w(x_i$-$x)$ is a weight function which addresses the effect of distance between the two points. The weight function should decrease monotonically with the increase of the distance, i.e. when a point is further away from the point x_i, its influence on point x_i should become less

significant. The weight function assumed here is a standardized Gaussian function as shown in Eq. (2.20), where $\sigma_1$is the standard deviation and is decided by the influence length l. From the property of Gaussian function, when x_i-x is beyond (-3 σ_1, 3 σ_1), $w(x_i$-$x)$ is almost zero as shown in Figure 2.5. We set $\sigma_1=l/6$ in the simulation.

$$w(x_i - x) = \exp\left(\frac{-(x_i - x)^2}{2\sigma_1^2}\right) \tag{2.20}$$

From Eqs. (2.15-2.18), the pressure decrease (increase) of a given point x_i due to a higher (lower) neighboring point will be compensated by the pressure increase (decrease) of this neighboring point due to point x_i. Thus the requirement of the global equilibrium is satisfied.

2.2.3 Local material removal rate (MRR)

With modified pressure P^* at point x_i on the wafer surface, Archard's law (1953) can be used to get the average MRR of the wafer at point x_i during the time step Δt.

$$MRR(x_i) = C_w \cdot P^*(x_i) \tag{2.21}$$

The total thickness removed from the wafer surface at point x_i during the time step Δt is computed by

$$\Delta Z_w(x_i) = MRR(x_i) \cdot \Delta t \tag{2.22}$$

By updating $Z_w(x_i, t_0 + \Delta t) = Z_w(x_i, t_0) - \Delta Z_w(x_i)$ for every time step, a time history of the wafer profile then can be obtained.

2.2.4 Simulation process at die scale

In order to obtain the wafer profile evolution at the die scale, a two-scale modeling approach combining the effects due to die scale profile and those due to feature scale pattern structures are used. In part A, the die scale (global) profile is extracted to calculate the pressure distribution along the wafer while neglecting the detail pattern structure at the

feature scale. In part B, further pressure re-distribution is incorporated due to the finer feature scale structure. The simulation process flow is shown in Figure 2.6 and may be described as following.

Part A – Die Scale

1) The global profile at die scale is obtained by extracting the wafer thickness on the up area and neglecting the pattern structure at the feature scale (as shown in Figure 2.7);
2) The local contact pressure distribution is evaluated based on the global profile using Eq. (2.11);
3) Due to the surrounding topography effect, the local contact pressure from step 2) is redistributed using Eqs. (2.18-2.19) by assuming that the pad contacts with the wafer up area everywhere during the polishing process.

Part B – Feature Scale

4) The final effective local contact pressure is obtained by re-distributing the local contact pressure in step 3) due to the feature scale structure effect. Eqs. (2.15-2.16) are used when the pad does not contact with the down area at the feature scale. Eqs. (2.18-2.19) are used when the pad contacts with the low area.
5) The local material removal rate is calculated from the effective local contact pressure using Eqs. (2.21). The wafer topography is updated based on the local MRR;
6) The updated wafer profile is applied and the procedure is repeated for the next time step (as shown in Figure 2.6).

The model is developed to evaluate the wafer profile evolution by integrating the pattern density and the die scale profile. It can be extended to investigate the step height reduction and dishing at the feature scale by considering the global profile used in Part A as a flat surface.

The pad topography plays an important role on the MRR. It was found that MRR drops rapidly if the pad is not conditioned (Stein et al., 1996). The pad wear effect on the wafer surface evolution is not considered in this thesis, and will be investigated in the future.

2.3 Model Verification

In this stage the model predictions of die scale global step formation due to variations in feature scale parameters (e.g., pattern density, line width, pitch) are validated against experimental observations in Ouma et al. (2002). The experiment is done by an Ebara polisher with IC1000 pads used over a sub-pad with a fixed thickness. The mask layout of one die used in the experiment is shown in Figure 2.8. It is 20mm×20mm and discretized into many blocks. Each block is 4mm×4mm with different pattern structures. The prefix D denotes pattern density. Each density structure consists of vertical lines and spaces of 100μm pitch (the length of the line width and the space width). For example, D10 means that the line width is 10μm and the space width is 90μm. The prefix P denotes pitch. The density for each pitch structure is fixed at 50% (equal line width and space width). For example, P20 means both the line width and the space width are 10μm each. Along the line L3 and L4, the pattern density gradually increases from block to block. The step pattern density is defined along the line L5. L6 has a constant pattern density but the pitch length for each block is different. The pre-CMP wafer has a patterned surface with the initial step height (the height difference between up area and down area) 0.6μm. In their experiment, the thickness was measured on the up area (line) and down area (space) at several locations.

2.3.1 Parameter estimation

In the simulation, the nominal pressure is set at 34kPa under the assumption that the nominal pressure applied to each die across the wafer is constant. The properties of pad asperities given in (Stein, 1996) are used in the simulation. The parameter values for pad asperity properties are presented in Table 2.1. The distribution of pad asperity heights is characterized by Pearson IV distribution. The procedure used to estimate the distribution of pad asperity heights can be found in Wang et al. (2005) and Johnson (1970). The Young's modulus E_p for IC1000 pad is assumed to be 29 MPa (Baker, 1996).

Other parameters including at l (the influence length), C_w (the coefficient

proportionality), α (the pad bending factor), and critical contact height (H) needed in the simulation are estimated as following.

1) The coefficient C_w

The coefficient C_w in Eqs. (2.9) and (2.21) is related to the relative velocity between the wafer and pad as well as the pad and wafer material properties. In the model, the MRR is proportional to the local contact pressure by the coefficient C_w. Thus, if the local MRR and local contact pressure are known, C_w can be estimated.

For a blanket wafer CMP, the contact pressure can be easily calculated by Greenwood and Williamson's model by assuming the wafer surface is smooth. For a pad with given statistical parameters in Table 2.1, the ratio of the real contact area to the nominal contact area is about 0.8% using Eq. (2.8). Thus the real contact pressure calculated is about 4.2 MPa using Eq. (9a) when the nominal pressure is 34kPa.

The MRR estimation for a blanket wafer surface can be found in Ouma (1998) and Xie et al. (2006). Here the MRR is simply estimated as the average wafer thickness reduced during a unit time in the experiment. From the experimental data for L5 at 29 and 89 seconds of polishing, the MRR is estimated as the mean thickness reduced from the wafer profile at 29 second to the wafer profile at 89 second for the corresponding locations. The mean MRR turns out to be 318 nm/min approximately. So, the coefficient C_w is estimated as 1.25×10^{-9} μm/sec/Pa.

2) Influence length at feature scale (l_f) and at die scale (l_d)

The influence length is defined as a distance over which the pad bends. At the feature scale, the pad bending is influenced by the local pattern structure. On the mask layout shown in Figure 2.8, the pattern structure is periodical in each block. Therefore, the feature scale influence length l_f may be assumed to be the pitch length. In Part B of the simulation where the feature scale is considered, the influence length l_f is set to be the pitch length.

As the polishing time increases, the variation of die scale (global) profile will be generated since the MRR is different in different regions of the wafer due to variations in

pattern structures. Then the pad also bends to conform to the die scale (global) profile. The influence length at the die scale can be characterized by the deformation length within which the pad surface will deform to follow the deformation of a loaded point. In other words, the MRR at a given point is influenced by its surrounding topography within this deformation length. The deformation length is defined as the planarization length in Ouma (1998). The approach to obtain this length was also investigated there. Therefore the pad influence length (l_d) in Part A of the simulation is approximated as 3mm, the average planarization length calculated from Table I in Ouma, et al. (2002).

3) The pad bending factor α

When the pad contacts with a patterned wafer, the contact pressure at a given point not only depends on the pad deformation at that point, but also depends on the pad deformation at the neighboring points. The zone of influence, over which the neighboring points affect a given point, has already been considered by the influence length. But the extent or magnitude of the influence of the neighboring points for a given location is governed by the pad bending factor. The estimation of the pad bending factor can be obtained by the following.

For the wafer profile evolution (actually the step height reduction) simulation at feature scale, the influence length can be set as the pitch length and the coefficient C_w can be estimated by the blanket wafer polishing. Only one parameter remains to be estimated. It is the pad bending factor. The feature scale model prediction (step height reduction) is fitted to a single experimental data point to estimate the value for the pad bending factor.

In the simulation for the experimental data in Ouma et al. (2002), the step height reduction vs. time for the center point in each block on L5 may be used to estimate the pad bending factor since the global pad bending has a smallest effect there. From the experimental data for L5, we choose the data point at the location of 10 mm. The step height at 29 second for this location is about 0.33 μm, it reduces to about 0.021 μm. The pattern density is 0.3 and the pitch length is 100 μm at this location. Using the feature scale

simulation to evaluate the step height reduction at the selected point, the pad bending factor turns out to be 0.55×10^{12} N/m^3 if C_w is set to be 1.25×10^{-9} μm/sec/Pa.

4) The critical contact height H

The critical contact height H is used to decide whether the down area of the wafer starts to be polished. It is different for different pattern structures and different applied pressures for a specified pad. In Cu CMP, dishing occurs due to the local pad bending. The saturation dishing depth (the asymptotic value of dishing for long time) for a non-selective slurry and elastic pad property is assumed to reflect the maximum pad bending depth. So it may be assumed to be the critical contact height H. The values for each pattern structure are obtained from Laursen et al. (2002).

2.3.2 Comparison of simulation results to experimental data

The values for parameters used in the simulation are summarized in Table 2.2. Figure 2.9 shows the model predictions (denoted by line) compared to the experimental data (denoted by points). The solid line and the solid points are the data for 29 seconds of polishing. The dashed line and the open points are for 88 seconds of polishing. The prediction error is also given with the root mean square (RMS) in Table 2.3.

From Figure 2.9 and the prediction error shown in Table 2.3, it is observed that the simulation reliably captures the effects of the pattern density on the post-CMP wafer surface. At the region with lower pattern density, the up area thickness reduced faster. At the region with higher pattern density, the up area thickness reduced slower. It is interesting to note that the predicted MRR results are a little faster than the experimental measurement at 88 second. Pad wear is a likely cause of this discrepancy. No pad wear is considered in our model. It is also noted that the low area surface for 29 second from simulation slightly underestimates the experimental data. This may be due to the initial roughness of the pad. Before the step height reaches the contact height H, at which the pad contacts with the wafer surface completely, some asperities with small radius and high height may have already contacted the low area

and polished the low area in the experiment. In our model, this situation is simplified.

2.4 Parametric Study

A multi-scale model integrating the effects of both die scale and feature scale profiles is developed and is verified against experimental data in section 2.3.2. Based on this model, impacts of several parameters, such as pad roughness, the pad global influence length l_d and pad bending factor α are schematically studied using the wafer profile shown in Figure 2.10. There are two different pattern structures on the wafer. The pattern density in the center zone (pitch length is 100 μm) and the edge zones are 0.3 and 1.0 respectively.

1) Effect of pad roughness on mean material removal rate

In this study, the parameters in Table 2.1 are used and the standard deviation for pad surface properties is varied. The nominal pressure $\overline{P}$, coefficient C_w, the influence length l_d and the pad bending factor are fixed during the simulation. It is assumed that the pad contacts with the down area of the wafer surface. Figure 2.11 shows the mean MRR during 1 minute of polishing for pads with different standard deviation values. The simulation results show that a pad with a higher standard deviation provides a larger MRR. For a pad with a standard deviation of 25 μm, the MRR is about 2 times of that obtained from the pad with a standard deviation of 5 μm. The standard deviation of pad asperity heights usually indicates the pad surface roughness. A higher standard deviation means a rougher pad surface. A rougher pad has a smaller real contact area with the wafer. This results in higher real contact pressure. Thus, a higher MRR is obtained by such a pad. During the CMP process, a freshly conditioned pad usually produces a high MRR. However, it drops rapidly with time if the pad is not conditioned. The mean MRR decay has been observed by experimental investigations in Stein et al. (1996). This phenomenon can be explained by this model. The initially higher pad asperities in contact with the wafer are worn down with continued polishing. The pad surface becomes smoother and the standard deviation of pad asperity heights will get smaller

with the polishing process if the pad is not conditioned. With the evaluation of the pad surface evolution, the MRR decay can be simulated by the model.

2) Effect of the die scale influence length l_d on global planarity of post-CMP wafer surface

The influence length at feature scale l_f only affects the local planarity. The effect of the influence length on the global planarity is studied by changing the die scale influence length l_d in the simulation. The pad bending factor is fixed as 0.3×10^{12}N/m^3. Figure 2.12 presents the wafer profile after 10 minutes of polishing using different influence lengths l_d. It is found that a longer influence length l_d results in a more uniform post-CMP wafer profile. The standard deviation of the wafer thickness is used to describe the planarity of wafer surface. The post-CMP profile with an influence length of 300 μm has a standard deviation 20% less than with the influence length of 100 μm. If we assume the pad to be elastic (Winkler) foundation, the influence length indicates that a given spring is affected by the neighboring springs within this distance. A pad with a larger influence length means that more springs affect each other. The MRR at a given point will be affected with surrounding topography within a longer distance. If the pad bending factor is spatially uniform, the total pad bending effect will be higher for a pad with a longer influence length. It can be conjectured that the polished wafer surface will be more uniform with a longer influence length. The influence length with 0 indicates that those springs become uncoupled. When they are pressed onto the patterned wafer surface, the force applied at a given point only depends on the deformation of the corresponding spring and is not affected by its neighbors. Therefore, the material removal rate at a given point is not affected by its surrounding topography. The MRR at a high point will not be enhanced by its surrounding low area, while the MRR at low point will not be reduced by its surrounding high area. The post-CMP wafer profile has a less planarity.

3) Effect of the bending factor α on global planarity of post-CMP wafer surface

The effect of the bending factor on the global planarity of post-CMP wafer surface is

investigated by keeping the influence length l_d constant as 300 μm. Figure 2.13 shows the wafer profile after 10 minutes of polishing with different bending factors. It may be observed that the larger bending factor gives better global planarity if l_d is constant. The post-CMP profile with the bending factor of $0.3\times1012N/m^3$ has a standard deviation 34% less than with the bending factor of 0. The bending factor describes the pad bending ability. The bending factor with a larger value which is typical for a hard pad indicates that the pad is difficult to bend. For such a pad, the higher area on the wafer effectively shades its neighboring lower areas and releases the load from the lower area. Thus the MRR is enhanced at higher area and reduced at lower area. The wafer surface will be polished more uniformly. In order to get a better planar surface, a pad with higher bending factor should be used. The pad bending factor is significantly influence by the pad surface microstructure. The approach to manufacture such a pad can be found in Fu et al. (2003).

Both the bending factor and influence length affect the post-CMP wafer surface. But they contribute in different ways. The bending factor considers the height difference effect while the influence length considers the zone of influence of a given point from its surrounding topography.

2.5 Summary

A multi-scale model is proposed to evaluate the wafer surface evolution during a CMP process. The interface pressure between a patterned wafer and a rough pad is evaluated based on the work of Greenwood and Williamson (1966). Two pressure re-distribution methods are proposed to take into account the effects of surrounding topography due to the pad bending. The model predictions are verified against experimental data of Ouma et al. (2002). The estimation procedure for the parameters used in the model is discussed. The effects of pad roughness, die scale influence length, and the bending factor on the wafer surface evolution are studied. It is observed that a rougher pad gives a higher material removal rate. Both the influence length l_d and the pad bending factor α contribute to the

planarity of the wafer surface. The higher values of the influence length and bending factor give better global planarity of the post-CMP wafer surface.

Figure 2.1: Global step height generated due to the different pattern density.

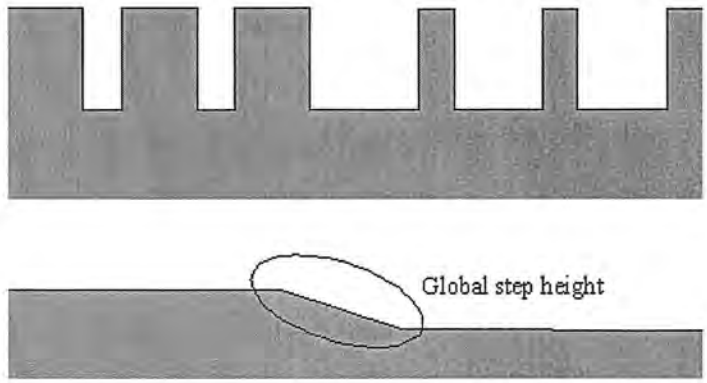

Figure 2.2: Illustration of the Greenwood and Williamson model (1966).

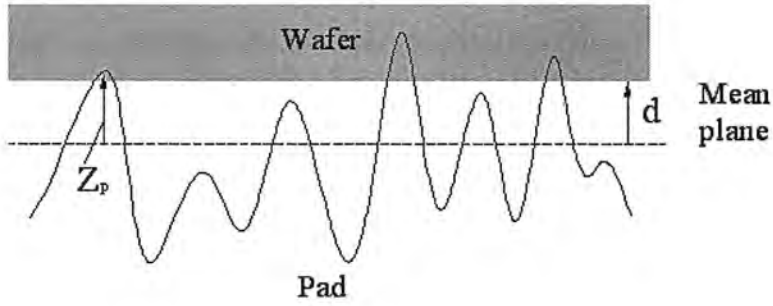

Figure 2.3: Schematic of the contact model between a rough pad and a patterned wafer.

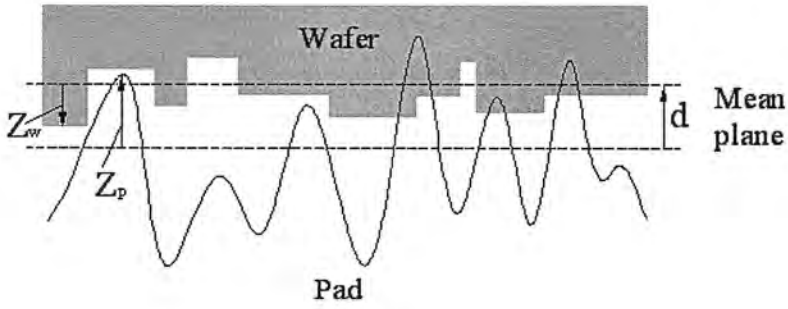

Figure 2.4: Schematics of the pattern wafer/pad contact interface: (a) pad contact with wafer completely (b) pad not contact with the down area of wafer.

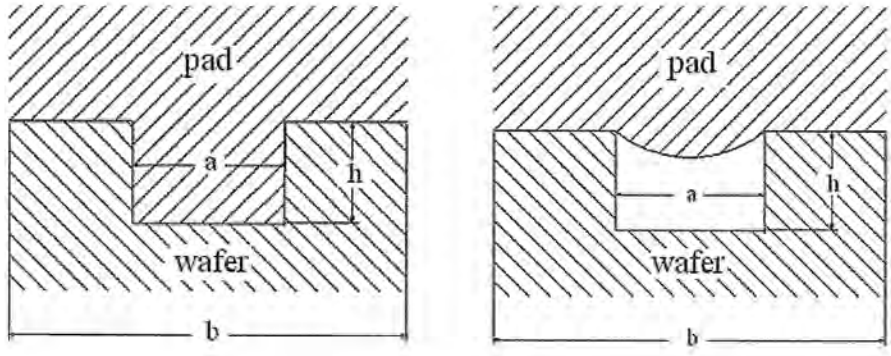

Figure 2.5: Profile of standardized Gaussian function.

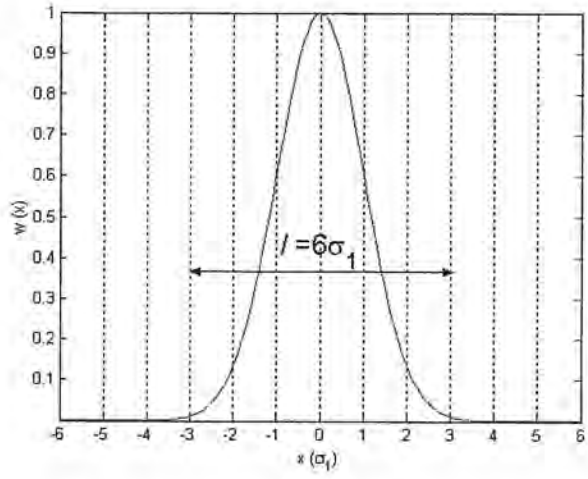

Figure 2.6: The simulation process flow.

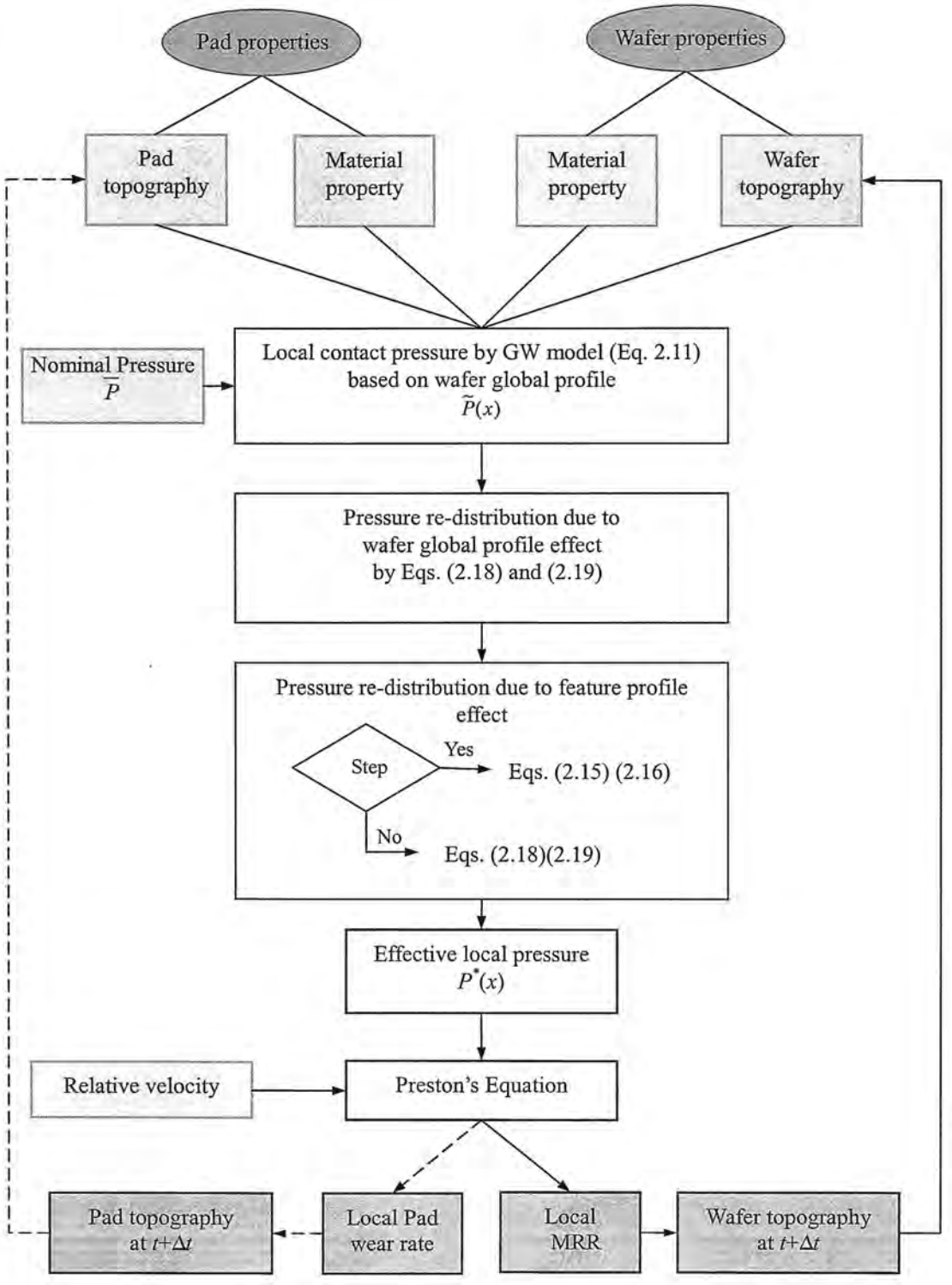

Figure 2.7: (a) Wafer profile (b) Extracted global profile at die scale.

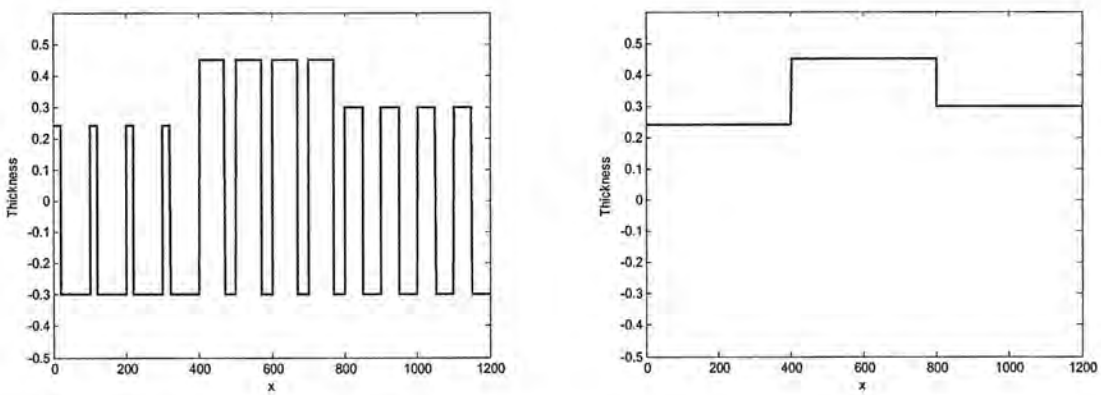

(a) (b)

Figure 2.8: Layout of the oxide CMP characterization mask. (Ouma et al., 2002)

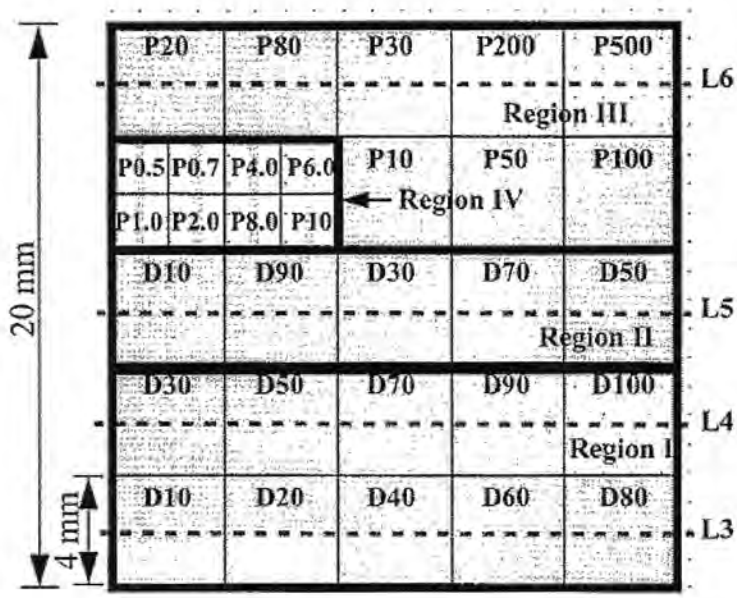

Figure 2.9: Predictions for up area and down area across line L3, L4, L5 and L6 (Ouma et al., 2002) respectively.

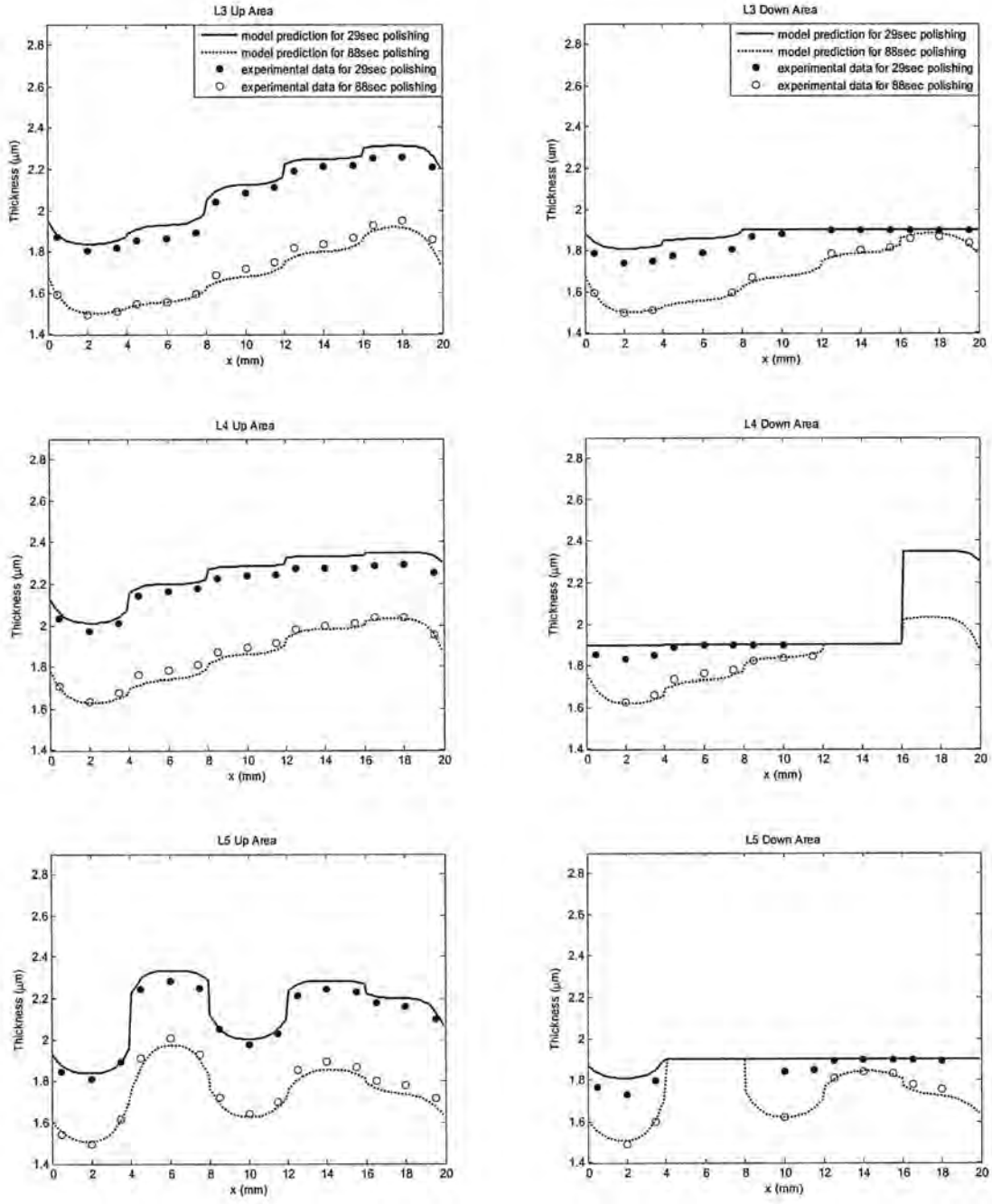

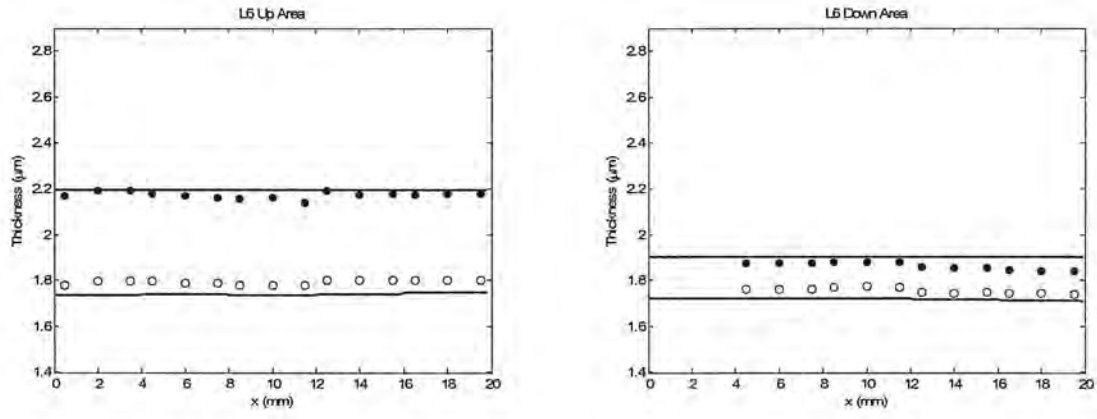

Figure 2.10: The wafer profile before CMP.

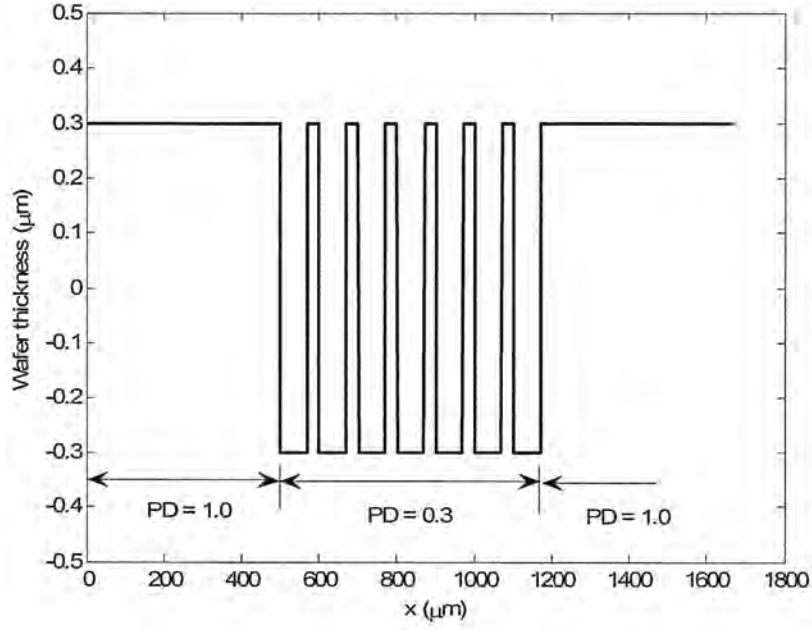

Figure 2.11: MRR with the pad roughness.

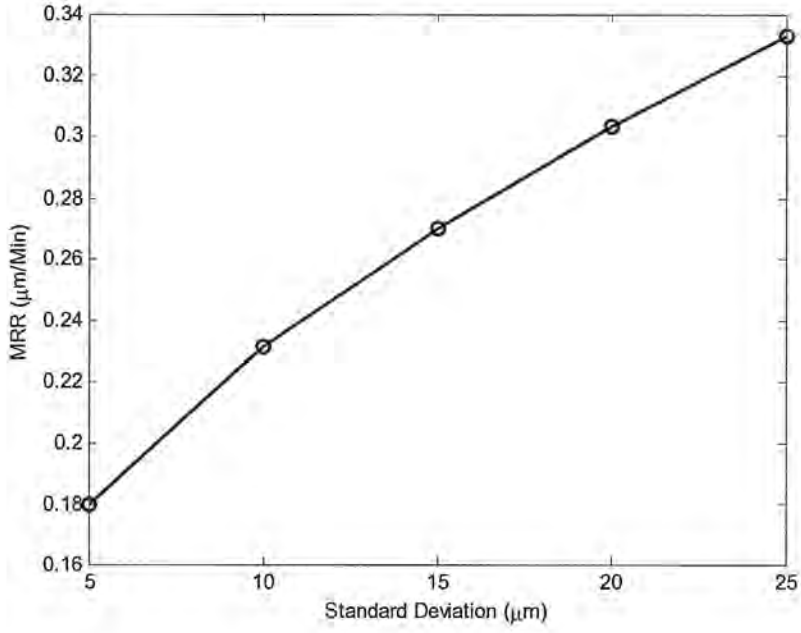

Figure 2.12: Wafer profile after 10 minutes of polishing with different influence.

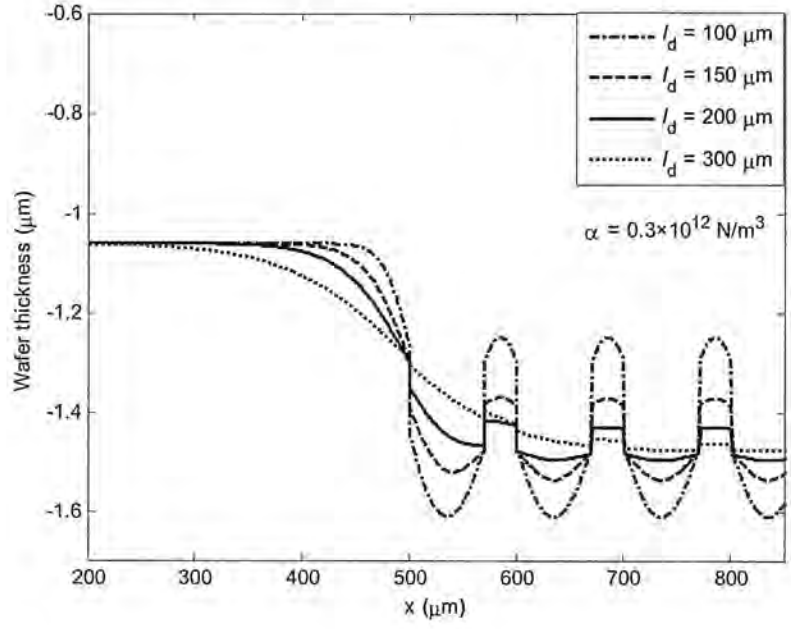

Figure 2.13: Wafer profile after 10 minutes of polishing with different bending factor.

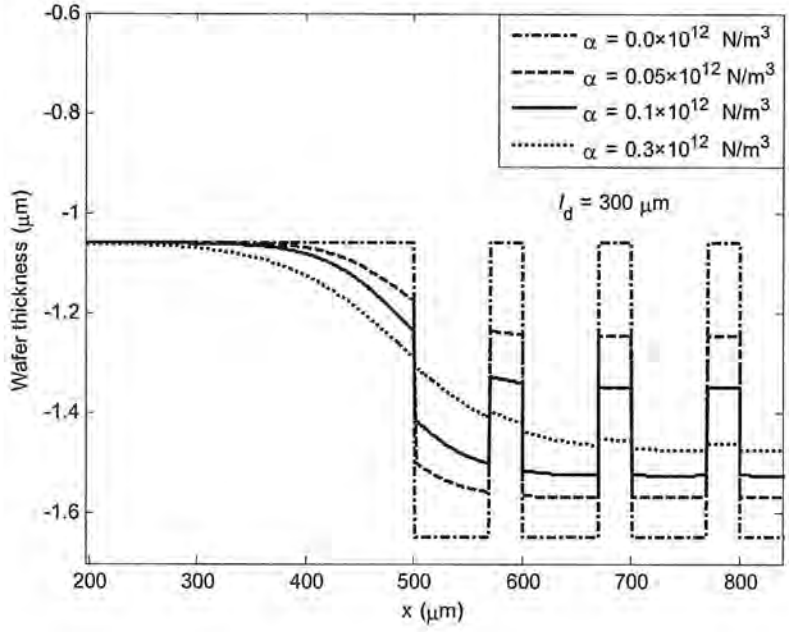

Table 2.1: Parameter values for pad asperities height.

Parameters	Values
Asperity Radius (R_p)	50μm
Standard deviation of asperity height(σ)	15.625μm
Skewness (γ)	-1.25
Kurtosis (β)	6.875
Asperity density (η_s)	$2\times10^8/m^2$

Table 2.2: Parameter values for die scale simulation.

Parameters	Values
Coefficient C_w	1.25×10^{-9} μm/Pa/sec
Die scale influence length l_d	3 mm
Feature scale influence length l_f	Pith length
Pad bending factor α	0.55×10^{12} N/m^3
Critical contact height H	0.11, 0.068, 0.1, 0.082, 0.09 μm

Table 2.3: Prediction error.

Line No. on wafer	RMS Prediction Error (Å)
L3	396
L4	418
L5	434
L6	416

Chapter 3: Effect of Particle Size Distribution on Material Removal Rate for Chemical Mechanical Planarization

The model in chapter 2 assumes that the pad and wafer contact directly without considering the slurry particles. However due to the fact that the pad is much softer than the wafer and the abrasive particles, the contacts between wafer and abrasive particles contributes the most to the material removal rate (MRR). This has been demonstrated by Larsen-Basse et al. (1999) in an experimental study on possible wear mechanisms. The abrasive particles trapped in the wafer-pad contact region are indented into the wafer surface and shear off the wafer surface material when the particles slide across the wafer surface. Researchers have developed MRR models based on the abrasion of particles (Luo et al., 2001; 2003; Fu et al., 2001; Zhao, 2002; Wang et al., 2005). They found that the accurate predictions of the force applied on the active particles, the material removed by a single active particle, and the number of abrasive particles involved in abrasion (the active particle) were important to investigate the MRR.

Luo et al. (2001, 2003) assumed that all of the slurry particles within the volume occupied by the pad asperities are entrapped in the contact areas between the wafer and pad asperities, however only a fraction of these particles were active particles. The number of active particles depends on the pad topography and the particle size distribution as well as the wafer and pad material property. In this model, the pad asperities were assumed to have the same height instead of a random height distribution described in Chapter 2. The force applied onto a particle is assumed to be the local pressure multiplied by the cross section area of the particles for a soft pad which is typical case in CMP. The material removed by a single particle is calculated based on the indentation-sliding model.

Fu et al. (2001) studied indentation due to spherical and sharp particles. The force carried by a single active particle is determined by the beam bending theory.

Zhao et al. (2002) proposes a model which is different from the Luo's model in: i) the estimation of active particle number. They assumed that most particles were squeezed away as the pad asperity approaches the wafer surface and only a single layer of slurry particles entrapped in the wafer-pad contact interface. However, all these entrapped particles were assumed to be active particles. In the model, the pad asperity has the property as in Chapter 2. But the particle size is uniform; ii) the material removed by a single particle, actually the indentation depth in the paper. They assumed that the particle contacts with the pad elastically and with the wafer plastically. The indentation depth into wafer can be obtained by applying the force equilibrium (the elastic contact force with the pad equals to the plastic contact force with the wafer) of the particle and by equaling the total indentation depth (the indention depth into the pad and the indentation depth into the wafer) to the dimension of particle. Then the material removed by a single particle was calculated in the same way in Luo et al. (2001).

Wang et al. (2005) extended the model by taking into account the pad wear during the CMP process.

In this chapter, the model developed in Chapter 2 is extended to account for the effects of abrasive particles. The wafer material removal is also assumed to be primarily due to the abrasive wearing of abrasive particles. Different from the models mentioned above which investigated the mean MRR of the whole wafer surface, this model attempts to determine the MRR at each location on the wafer surface so that the wafer surface evolution can be obtained. In order to achieve this goal, a small region on the wafer surface is focused, and the three variables needed to determine include: i) the pressure applied at this small region, ii) the number of the active particles which slide over this small region during each time step, and iii) the material removed by a single particle under the applied pressure when it plows across the focused small region on the wafer surface. The effective contact pressure

at any location on the wafer surface has been investigated in Chapter 2. Since the particles are smaller compared with the pad asperities, it is reasonable to assume that the particles do not affect the contact pressure between the wafer and pad. In this chapter, the other two variables are to be determined. When all the three variables are obtained, the wafer surface evolution can be obtained.

3.1 Model Development

3.1.1 The number of active particles

The number of active particles plays an important role on MRR. Two different models to predict the number of active particles have been proposed (Luo et al., 2001, 2003; Zhao et al., 2002; Wang et al., 2005). They are briefly introduced in this section. Based on the model by Zhao et al. (2002) and Wang et al. (2005), an extending model is developed to consider the wafer surface roughness effect on the number of active particles.

Fig 3.1 shows the schematic of the wafer/pad/particle contact model in Luo et al. (2001, 2003). The pad asperities are uniformly distributed on the surface. All asperities have the same height and the spherical asperity tip radii are constant. When the wafer is pressed onto the pad, all asperities deformed equally with a contact area A, and all asperity heights decrease to a smaller value $\tilde{l}$. This model assumes that the total number of particles captured within the wafer-pad contact area is the number of the particle in the slurry with a volume taken by the deformed pad asperities. The volume of the deformed asperities $Vol_{asperities}$ is given by $A\tilde{l}A_oD_{sum}$, where A_o is the nominal contact area and D_{sum} is the asperity density denoted by η_s in chapter 2. If the slurry particle volume concentration is assumed to be χ, then the total volume of the particles captured in the wafer-pad contact region is $\chi\, Vol_{asperities}$. The average volume of a particle is given by $\frac{1}{6}\pi(D_{avg})^3$ (Luo et al., 2001, 2003), where D_{avg} denotes the mean particle size. After knowing the total volume of the particles captured in the

wafer-pad contact region and the average particle volume, the total number of particles captured in the wafer-pad contact region, n, is determined by

$$n = \frac{\chi \cdot Vol_{asperities}}{\frac{1}{6}\pi (D_{avg})^3} \tag{3.1}$$

However, not all these particles are active. When the wafer approaches the pad surface under the applied force, all particles within the slurry volume occupied by pad asperities are captured in the wafer-pad asperity contact area and then cluster together. Thus a gap may form between the wafer and pad asperities. Assuming the width of the gap is g, only those particles with a size lager than g are active and contribute to material removal. If the particle size distribution is given as $y(D)$, then the number of active particles is

$$n_{active} = n \int_{D>g} y(D)dD \tag{3.2}$$

The calculation of g can be found in Luo et al. (2001, 2003) for a rough pad with identical height asperities uniformly spaced.

Another method for estimating the active particle number by Zhao et al. (2002) and Wang et al. (2005) is quite different from that the one in Luo et al. (2001, 2003). Zhao et al. (2002) and Wang et al. (2005) argued that when a wafer is pressed toward a pad, most particles are squeezed away before the wafer comes to a fairly close distance (the maximum particle size in Wang et al., 2005) to the tip of asperities. Only a small portion of particles are captured by the contact area between the wafer and pad asperities. The motion of particles is schematically shown in Figure 3.2. In their models, Zhao et al. (2002) and Wang et al. (2005) assumed that the particles captured in the wafer-pad asperity contact area were all active and remained uniformly spaced as in the slurry. Hence, the total number of active particles depends on the total contact area between the wafer and pad and the particle concentration in the slurry.

According to the Greenwood and Williamson contact model, the total real contact area between a smooth wafer and rough pad is given by

$$A_{re} = A_o \pi \eta_s R^* \int_{Z_p - d > 0} (Z_p - d)\phi(Z_p) dZ_p \tag{3.3}$$

where A_o is the nominal contact area; d is the separation distance between the wafer surface and the pad mean plane; and Z_p is the height of pad asperity with a PDF $\phi(Z_p)$ as in chapter 2. Therefore, the total volume of the particles captured in the wafer-pad contact region is $\chi D_{max} A_{re}$. The total number of the particles captured in the contact area is thus given by

$$n_{active} = \frac{\chi D_{\max} A_{re}}{\frac{1}{6}\pi (D^3)_{avg}} \tag{3.4}$$

So far the above methods to calculate the number of active particles are based on the assumption that the wafer surface is smooth. In fact, a wafer surface is usually patterned. Wafer surface roughness is not negligible compared with the particle size, which is about 50 to 200 nanometer. Zeng et al. (2005) has introduced a function $f(D_{avg})$ to consider the wafer surface roughness effect on the total number of active particles:

$$f(D_{avg}) = PD + (1 - PD)\left(\frac{D_{avg}}{D_{avg} + h(t)}\right)^2 \tag{3.5}$$

where PD is the wafer pattern density, which is defined as the ratio of line width over the pitch length (line width and space width) and h is the step height of the wafer which can be used to describe the wafer roughness. From this equation, it is clear that $f(D_{avg})$ approaches to 1 when the mean size of particles is much larger compared with the step height, which means the effect of wafer roughness on the number of active particles is smaller when the particle size is larger. When the particle size is very small, the last square term in (3.5) approaches zero. Thus, more particles will be entrapped into the low area of the wafer. Hence, when both the wafer roughness and pad roughness are considered, the number of active particles is given by

$$n_{active} = \frac{\chi D_{\max} A_{re}}{\frac{1}{6}\pi (D^3)_{avg}} \cdot f(D_{avg}) \tag{3.6}$$

3.1.2 Material removal by a single particle

The material removed by a single particle is determined by the force applied onto the particle and the surface material property.

1) Estimation of the force applied onto the particle.

From the model in Chapter 2, the local contact pressure $P^*(x_i)$ has been evaluated. The force applied onto the particle then can be estimated from the local contact pressure based on the contact mode of the particle. If it is assumed that the particle concentration is small and the pad is soft, the active particles are in full contact mode as described in Bastawros et al. (2002). Therefore, the load carried by a particle with size D is given

$$F = \frac{1}{4}\pi D^2 P^*(x_i) \tag{3.10}$$

2) Material removed by a single particle

As shown in Figure 3.3, with a load F, the active particles are indented into the wafer surface and plough off the wafer surface material. Assuming the leading edge of the indentation of each active particle into the wafer surface undergoes a perfect plastic deformation, the load balancing equation is therefore given as

$$F = \frac{1}{2}\pi\left[\left(\frac{D}{2}\right)^2 - \left(\frac{D}{2} - \delta_w\right)^2\right]H_w \tag{3.7}$$

where H_w is the hardness of the wafer. Since the indentation depth (δ_w) is much smaller than the particle size, it is reasonable to approximate δ_w as

$$\delta_w = \frac{2F}{\pi H_w D} \tag{3.8}$$

When an active particle slides over the wafer surface, a trench will be generated and the material in this trench is pushed away. The cross-section area of trench is estimated by

$$\Delta S = \delta_w\sqrt{\delta_w D} = \frac{1}{D}\left(\frac{2F}{\pi H_w}\right)^{\frac{3}{2}} \tag{3.9}$$

When an active particle slides across the wafer surface across a distance Δx, the average volume of the material removed by the particle is given as

$$\Delta V_{(\Delta x)} = \Delta S \cdot \Delta x = \left(D^2\right)_{avg} \left(\frac{P^*(x_i)}{2H_w}\right)^{\frac{3}{2}} \cdot \Delta x \tag{3.11}$$

3.1.3 Material removal rate

Consider a small region with area $\Delta x \cdot 1$ on the wafer surface shown in Figure 3.4. Δx is the resolution for the simulation. It depends on the pattern structure on the wafer. 1 means a unit length along the direction of line. If the active particles are assumed to be uniformly spaced on the wafer surface, the active particle density is n_{active}/A_o. During a time step Δt, the number of particles which slide over this small region is given as

$$n_{(\Delta x,\Delta t)} = \frac{n_{active}}{A_o} v \cdot \Delta t \cdot 1 \tag{3.12}$$

The average material removal rate during Δt is given by

$$\begin{aligned} \overline{MRR}(x_i,t) &= \Delta Z_w(x_i,\Delta t)/\Delta t \\ &= \frac{\Delta V_{(\Delta x)} \cdot n_{(\Delta x,\Delta t)}}{\Delta x \cdot 1} \Big/ \Delta t \\ &= \frac{6\chi v}{\pi} \cdot \left(\frac{P^*(x_i)}{2H_w}\right)^{\frac{3}{2}} A_f \cdot \underbrace{\frac{\left(D^2\right)_{avg} D_{\max}}{\left(D^3\right)_{avg}} f(D_{avg})}_{\text{the effect of particle size distribution}} \end{aligned} \tag{3.13}$$

where v is the relative velocity between wafer and pad; A_f is the ratio of the real contact area to the nominal contact area as defined in Eq. (2.8). In calculating A_f, the effect of the slurry particles is neglected since their size is very small compared with the pad asperity heights.

After a time step Δt, the wafer thickness at point x_i is updated as

$$Z_w(x_i,t+\Delta t) = Z_w(x_i,t) - \overline{MRR}(x_i,t) \cdot \Delta t \tag{3.14}$$

Carrying out the same calculation for each location on the wafer surface results in an updated wafer surface profile at $t + \Delta t$.

The last term in Eq. (3.13) is related to particle size and its distribution. If the particle size distribution is characterized by a mean μ, a standard deviation σ, and a skewness γ, then

$$\left(D^2\right)_{avg} = \mu^2 + \sigma^2 \tag{3.15}$$

$$\left(D^3\right)_{avg} = \mu\left(\mu^2 + 3\sigma^2\right) + \gamma\sigma^3 \tag{3.16}$$

and

$$D_{\max} \approx \mu + 3\sigma \tag{3.17}$$

because more than 99.87% particles entrapped within the wafer and pad contact area are smaller than the size $\mu+3\sigma$ for a normal distribution. For a distribution with a positive skewness (Bare, 2000; Li et al., 2000), this proportion will be higher. Therefore,

$$\frac{D_{\max}\left(D^2\right)_{avg}}{\left(D^3\right)_{avg}} \approx \frac{(\mu+3\sigma)\left(\mu^2+\sigma^2\right)}{\mu\left(\mu^2+3\sigma^2\right)+\gamma\sigma^3} \tag{3.18}$$

The calculation procedure is summarized as following: at first, the contact pressure distribution along the wafer surface is calculated using Eq. (2.21) without considering the particle effect; then, the number of active particles which slide over the focused small region during a time step is determined using Eq. (3.12); next, the material removed by a single active particle is calculated when it slides over this region; and in the end , the material removal rate at any region on the wafer surface is evaluated and the wafer surface profile is predicted. Figure 3.5 shows the simulation process flow.

3.2 Model Verification

The experimental data presented in Ouma et al. (2002) are again used to validate the model with the particle effect considered. In this section, the model described in this chapter is referred as Model II while the model in chapter 2 is called Model I. Because information on particle size used in the experiment was not provided in Ouma et al. (2002), general particle size values are used here as an estimation. The mean particle size μ is ~100 nm; the standard deviation is ~20 nm; and the skewness is about 0 if the particle size distribution is

symmetric or very close to symmetric. The volume concentration of particles in the diluted slurry is ~1%. The pad mechanical properties and asperity properties are assumed to remain the same as those used in Chapter 2. The relative velocity between the wafer and pad is set to be ~0.6m/sec. The hardness of the wafer is ~2.2 GPa. The contact pressure calculated by Model I and all other parameters values (summarized in Table 3.1) are substituted into Eqs. (3.13-3.14). Then the wafer profile evolution can be obtained. Figure 3.6 shows the simulated results compared with the experimental data for L3, L4, L5 and L6 in Ouma et al. (2002). The prediction error (RMS) also given in Table 3.2.

3.3 Effects of Particle Size Distribution on MRR

The particle size distribution effect on the average MRR is reflected in the last term in Eq. (3.13). Thus the normalized average MRR can be used to study the effect of particle size distribution on the MRR in this section.

In general, the particle size distribution is assumed to be symmetrical normal distribution. However, a particle size distribution characterized by Courtesy of Millipore Corporation (in Bare, 2000) especially after particle agglomeration (Li et al., 2000) has a long right tail and is positive skewed. The influence of particle size distribution skewness is studied based on the model. Figure 3.7 shows the variation of normalized MRR with the particle size distribution skewness with a fixed standard deviation $\sigma = 20$ nm. As shown in Figure 3.7, the MRR decreases with the mean particle size if the skewness is close to zero. With a larger positive skewness (e.g., 2), MRR initially increases and then decreases with increasing particle size, indicating that there is an optimal particle size, where MRR reaches an optimal value. The existence of the optimal particle size has been shown in the experimental by Zhou et al. (2002). However, the physical implication of the observation that a positive skewness results in an optimal particle size still needs further investigation.

The effect of the standard deviation of a particle size distribution on MRR with a constant skewness $\gamma = 2$ is presented in Figure 3.8. With a constant skewness, the optimal

particle size is larger with a larger standard deviation. It is also seen that the MRR increases with an increasing standard deviation when the mean particle size is large. This indicates that a larger variability of particle size gives a larger MRR. However, wafer scratch may be caused by the presence of a few large particles (Bare, 2000).

The effect of wafer roughness on MRR is also studied based on this model. The wafer roughness effect originates its influences on the pressure distribution along the wafer surface and the number of active particles. Figure 3.9 shows the normalized material removal rate with the wafer step height without considering the particle size effect. It can be seen that the MRR does not change much if the wafer step height is small. However, the active particle number calculated by Eqs. (3.5) and (3.6) is significantly affected by the wafer roughness since the particle size is comparable with the wafer roughness. The wafer roughness effect on MRR via the active particle number is investigated for the small wafer step height. According to Eqs. (3.5) and (3.6), the number of active particles is smaller for a wafer with a larger step height since the ratio $f(D_{avg})$ decreases as the wafer step height increases. Hence, the MRR decreases with an increasing wafer step height. When the particle size is larger, the effect of wafer step height on MRR will be smaller since $f(D_{avg})$ is much smaller; then, the MRR will converge together if the particle size is larger enough. The normalized MRR as a function of particle size with different wafer step height is shown in Figure 3.10.

3.4 Conclusion

The model proposed in this chapter was based on the slurry particles indentation wear mechanism. The number of active particles and the force applied on them decide the material removal rate. Based on the two approaches in Luo et al. (2001, 2003), Zhao et al. (2002), and Wang et al. (2005), a third (modified) approach was proposed to estimate the number of active particles while considering the influences of both pad and wafer roughness. The number of active particles sliding over a focused region on wafer surface during a time step and the contact pressure applied on this region are calculated. The material removal rate on

this region is then obtained. By calculating the material removal rates for all regions on the wafer surface, the wafer surface evolution thus can be evaluated.

Particle size distribution significantly affects MRR. The model demonstrates that a positive skewness of particle size distribution results in an optimal particle size below which the MRR increases with increasing particle size and above which the MRR decreases with increasing particle size. With the present model, it is found that a larger standard deviation of particle size distribution gives a larger MRR when the mean particle size is large. It is also shown that MRR is smaller for a rougher wafer since the number of active particles is smaller. However, as the particle size increases, the effect of wafer roughness on MRR via affecting active particle number becomes smaller.

Figure 3.1: The schematic of contact model in Luo et al.(2001, 2003). x_{avg} and p are denoted as D_{avg} and y respectively in this chapter.

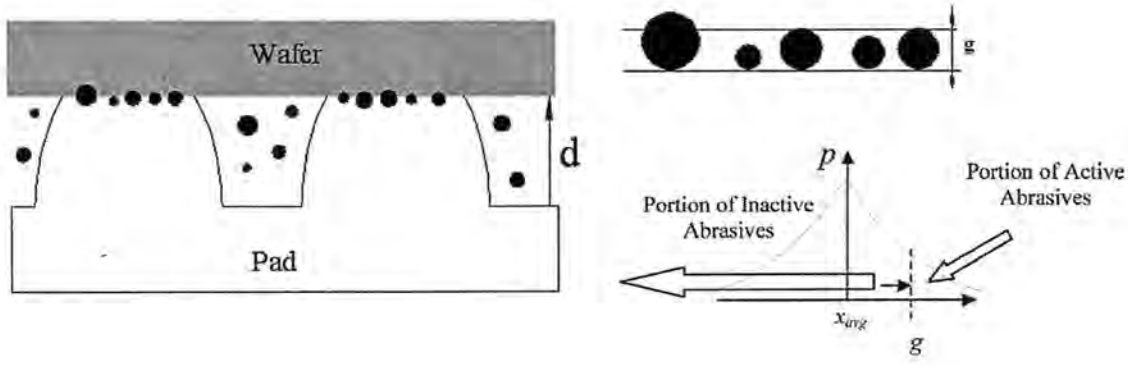

Figure 3.2: Particles motion schematic in CMP.

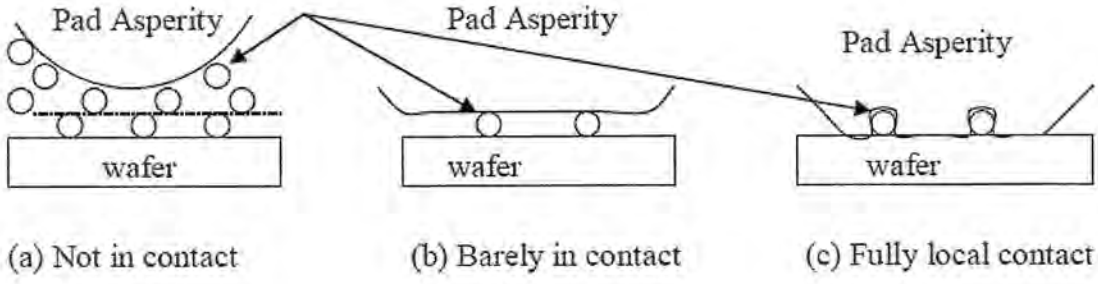

Figure 3.3: The indentation model of spherical particle.

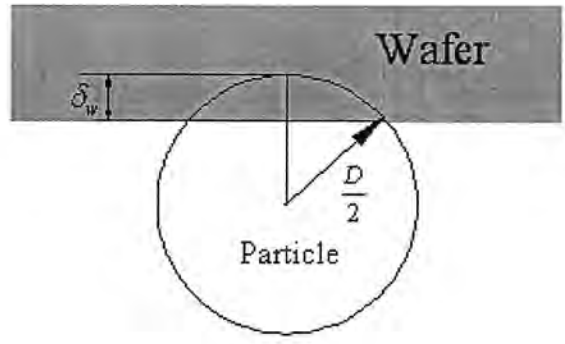

Figure 3.4: The schematic of material removal model (up view of wafer surface).

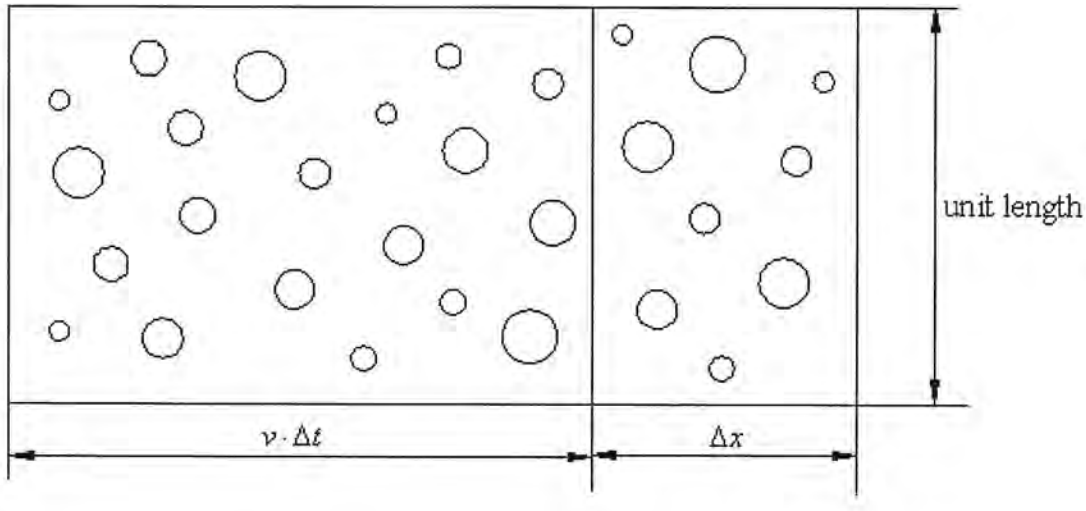

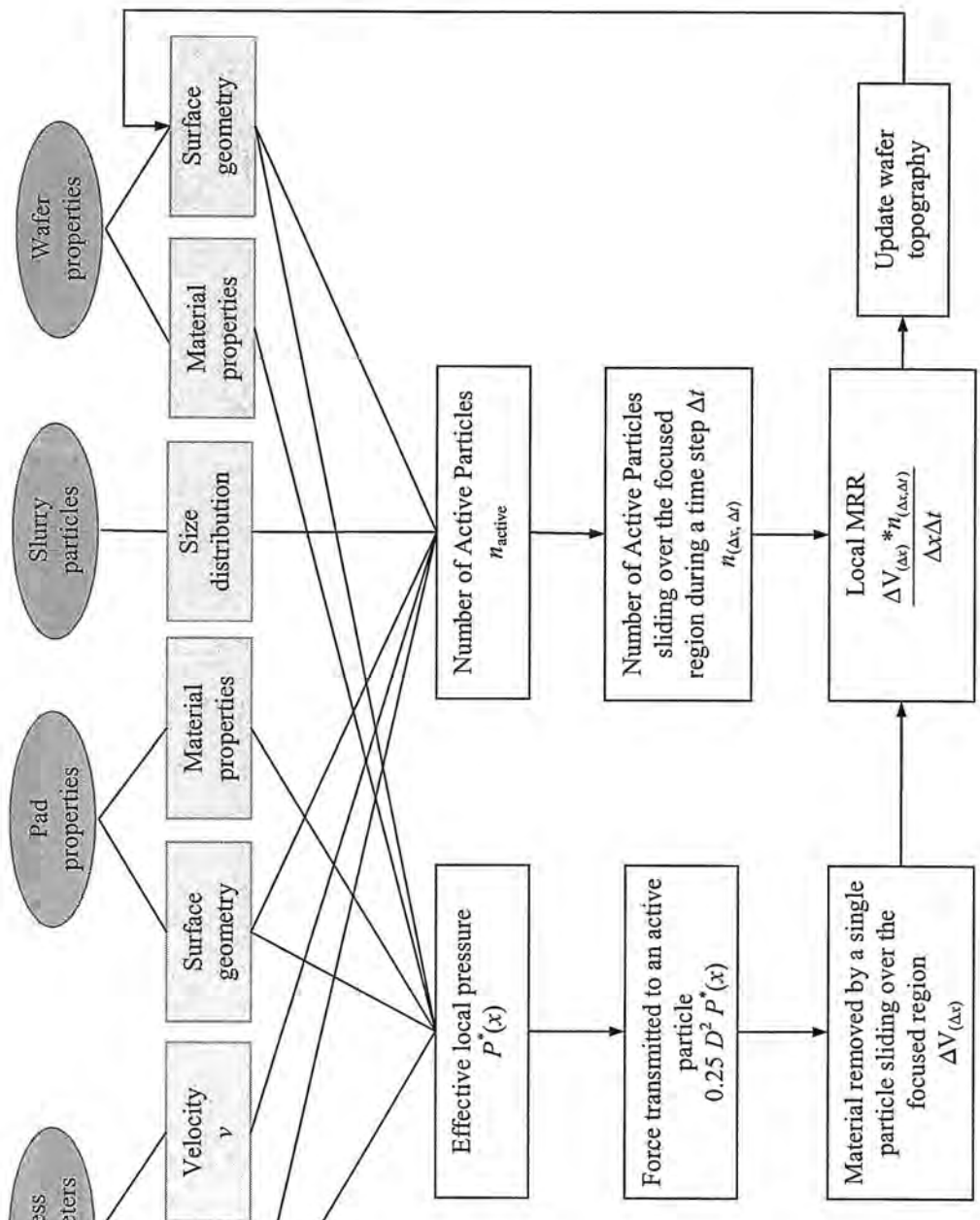

Figure 3.5: Simulation process flow

Figure 3.6: Prediction for up area and down area along line L3, L4, L5, and L6 respectively.

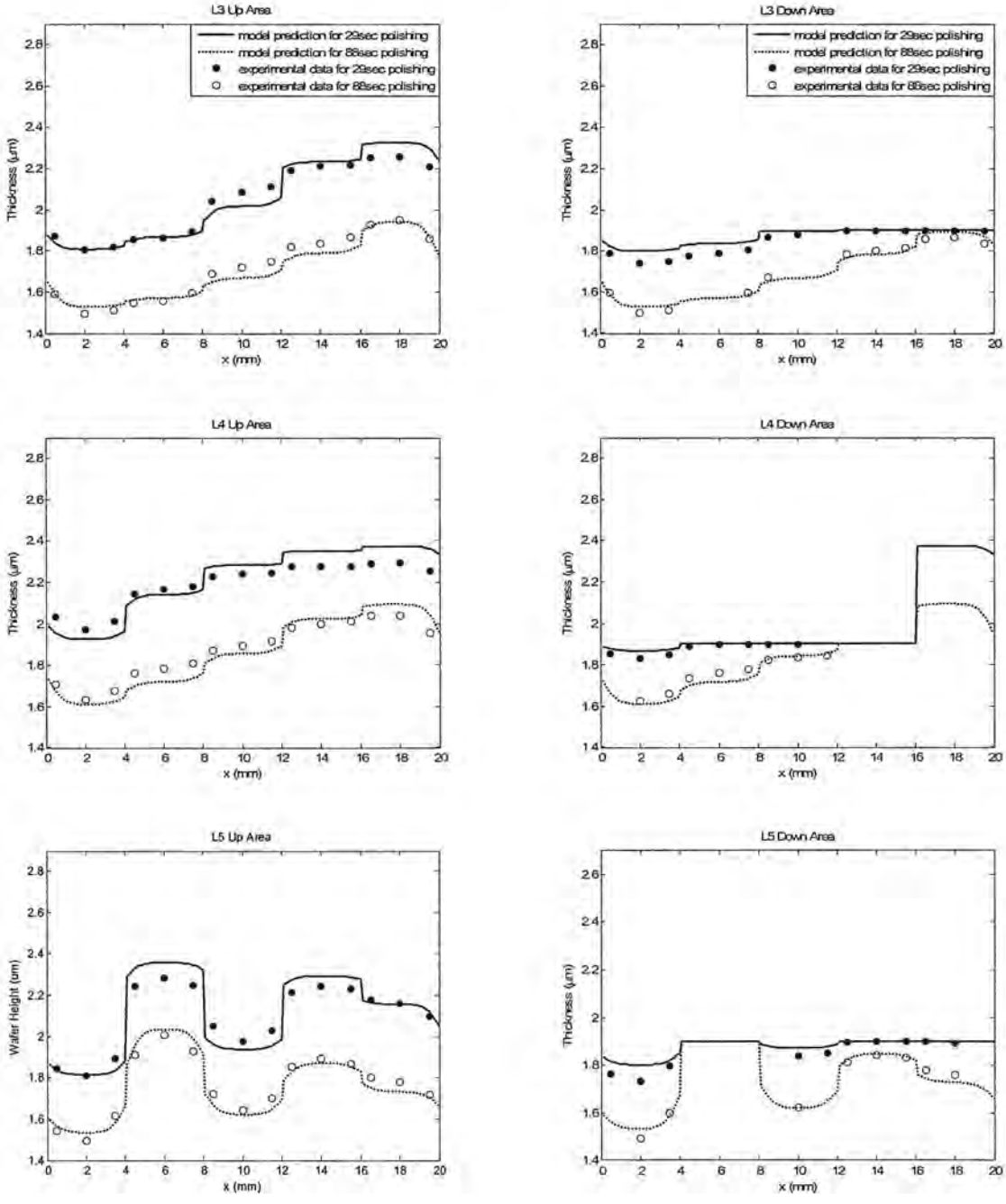

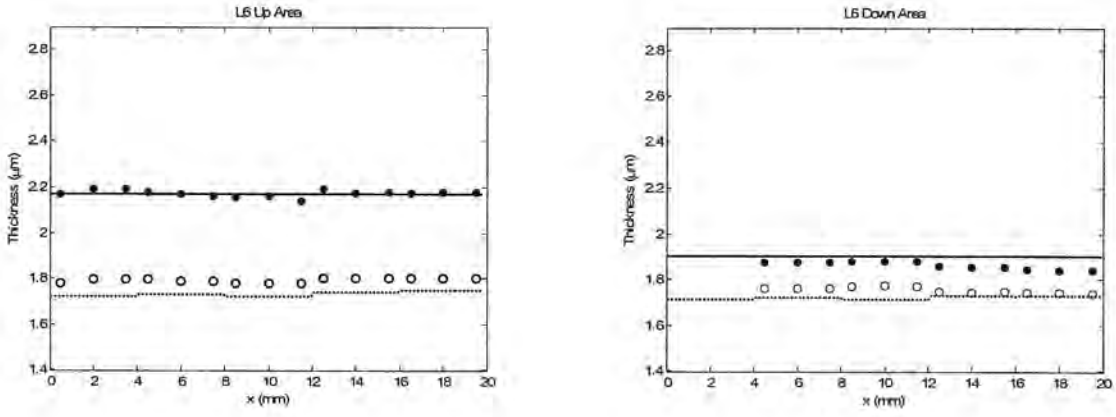

Figure 3.7: Effects of skewness of particle size distribution on MRR.

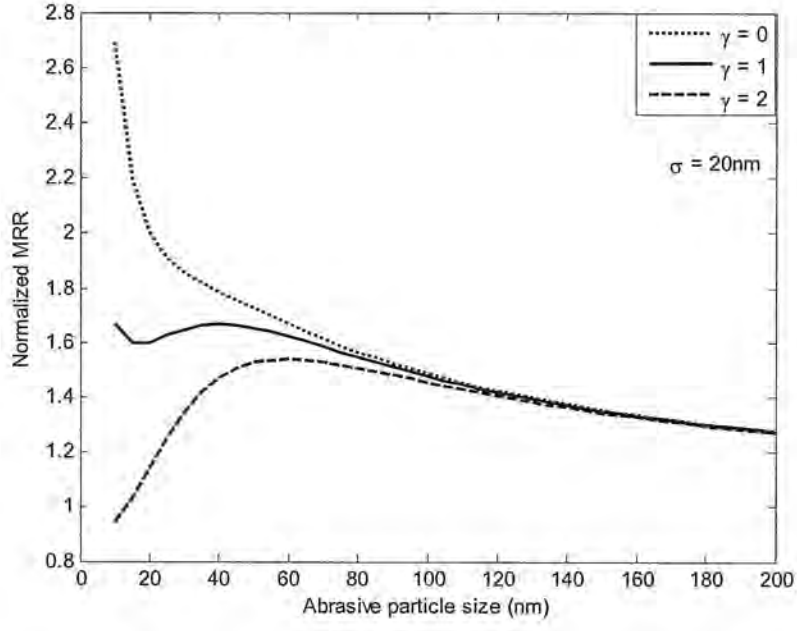

Figure 3.8: Effects of standard deviation of particle size distribution on MRR.

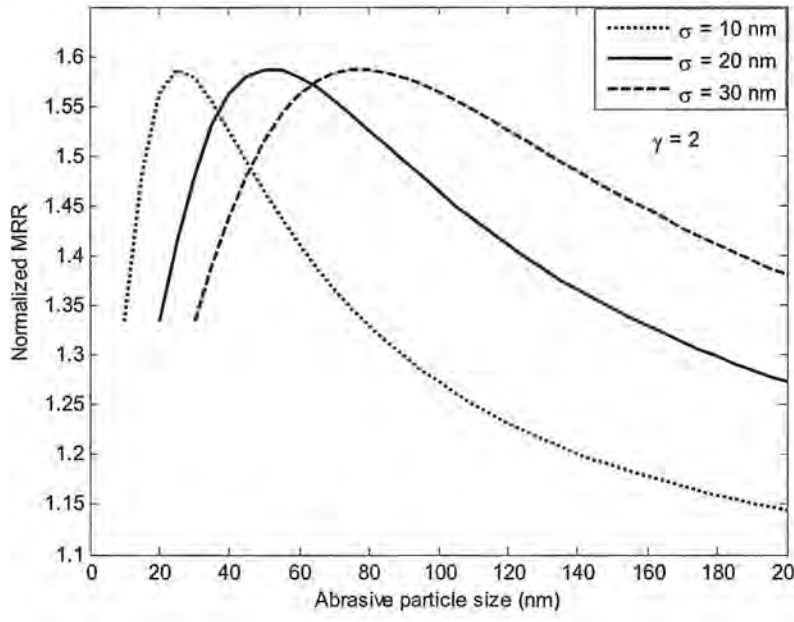

Figure 3.9: Wafer surface step height effect on mean MRR through pressure distribution.

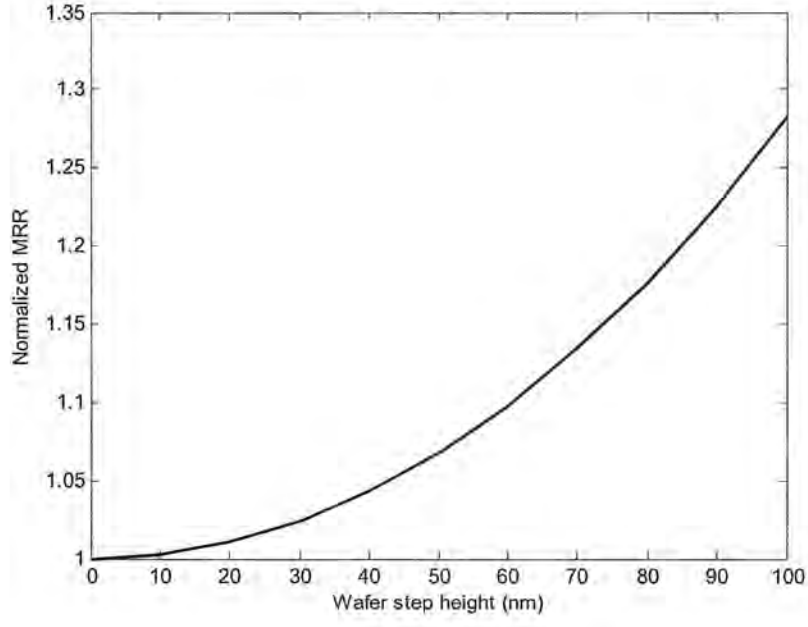

Figure 3.10: Wafer surface step height effect on MRR as a function of particle size.

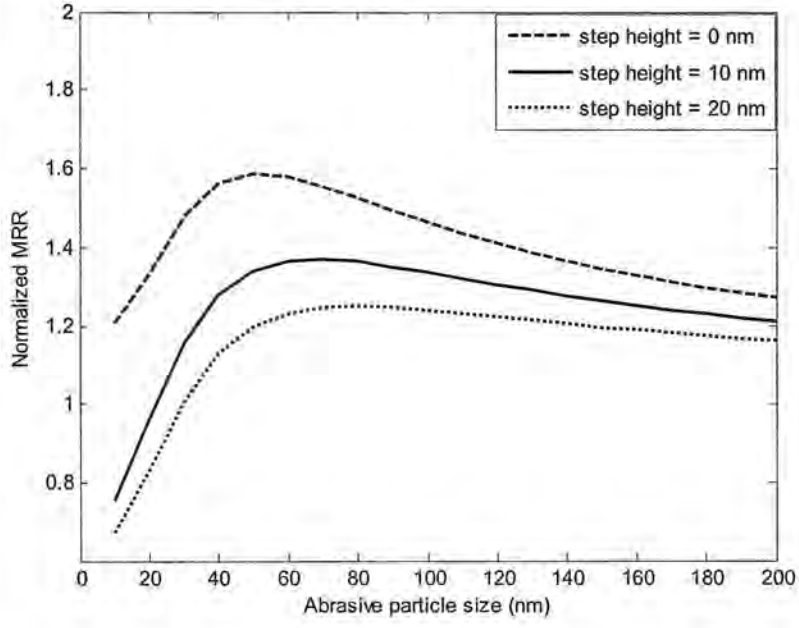

Table 3.1: Parameter values for the simulation

Parameters	Values
Particle volume concentration χ	1%
Mean particle size D_{avg}	50nm
Standard deviation of particle size distribution σ	20nm
Skewness of particle size distribution γ	0
Wafer hardness H_w	2.2GPa
Relative velocity v	0.6m/s

Table 3.2: Prediction error.

Line No. on wafer	RMS Prediction Error (Å)
L3	372
L4	480
L5	441
L6	399

Chapter 4: Conclusions and Recommendations for Future Work

Material removal rate in CMP is affected significantly by the pattern structures on wafer surfaces. Difference between material removal rates in different regions with different pattern structures generates wafer global thickness variation, which has a detrimental impact on subsequent process steps and also affects circuit performance. In this thesis, the mechanism of material removal rate and the pattern structure effects on material removal rate at die-feature scale in CMP was investigated.

In the first part of this chapter, the conclusions obtained in this study are summarized. In the second part, recommendations are provided on further work.

4.1 Conclusions

In chapter 2, we investigated the material removal rate distribution along a patterned wafer based on the assumption that the pad contacts with the wafer surface directly and the material removal rate depends on the local pressure linearly. Based on the work of Greenwood and Williamson, Model I was proposed to evaluate the local contact pressure distribution between a rough pad and a patterned wafer. For a patterned wafer, the pressure at a given point is affected by its surrounding topography due to pad bending. A neighboring point with a larger height difference and shorter distance from the given point has a more significant influence on the given point. Thus, two parameters (called "pad bending factor" and "influence length") were used to account for the surrounding topography effects through height difference and distance, respectively. The material removal rate distribution was evaluated from the pressure distribution by Archard's law. The wafer surface profile was updated after a time step. By reevaluating the pressure distribution and MRR distribution

based on the updated wafer profile, the wafer profile evolution was then obtained. The model was verified by experiment data and is able to reliably predict the wafer profile evolution.

In chapter 3, the material removal rate was investigated by extending Mode I to consider the slurry particles effect. It is assumed that the material is removed by the sliding indentation of slurry particles. Different from the previous models, our goal was to investigate the local MRR or the MRR distribution. Thus a small region on the wafer surface is focused. The contact pressure at this region was evaluated by Model I. When an active particle slides over this region, the material removed by this particle was obtained based on the assumption that the particle was in full contact modes (Bastawros et al., 2002) and the material in the indentation depth was detached completely. At the same time, the model evaluated the total number of active particles sliding over this region during a time step. After knowing the material removed by a single active particle and the total number of active particles sliding over the concerned small region during the time step, the material removed and the mean material removal rate at this location during the time step then were obtained. By calculating the MRR for all regions on the wafer surface, the wafer surface evolution thus can be evaluated. Based on the model, the particle size distribution effect on MRR was investigated. An optimum particle size was found when the particle size distribution has a larger positive skewness. The standard deviation was found to affect the MRR. When the mean particle size is larger, the MRR increases with the larger standard deviation. This indicates that more mixed particles provides a faster MRR.

4.2 Recommendations for Future Work

In Model I, the pad topography effect on the MRR was investigated by changing the standard deviation of pad asperity height. It was found that a smooth pad which has a small standard deviation of asperity height produced a slower MRR. In the simulation, we assumed that all pad asperities have spherical summits with constant radius. The fact is that the radius of asperities is random distributed. During the CMP process, the radius will becomes lager

which will also contribute to the MRR decay. This should be considered in the future work.

In chapter 2, Model I was developed for the die scale simulation. It can be extended to predict the step height reduction and the dishing with time at feature scale if we take the global profile as a flat surface. The verification for this function of the model should be done later.

In chapter 3, the active particles were assumed in a mode of full local pad asperity-wafer contact. There are many other possible contact mechanisms in the CMP such as no local-pad asperity-wafer direct contact and partial local-pad asperity-wafer direct contact in Bastawros et al. (2002). We will extend the Model II by applying other contact mechanism. From the model, we also found a positive skewness of the particle size distribution resulted in an optimum particle size. The fundamental reasons should be investigated.

References

Archard, J.F., (1953), "Contact and rubbing of flat surfaces," *Journal of applied physics*, Vol. 24, pp. 981-988.

Bajaj, R., Desai, M., Jairath, R., Stell, M., Tolles, R., (1994), "Effect of polishing pad material properties on chemical mechanical polishing (CMP) processes," In: *Advanced Metallization for Devices and Circuits Science, Technology and Manufacturability, Proceedings of the Materials Research Society*, Vol. 337, pp. 637-644.

Baker, A.R., (1996), "The origin of edge effect in chemical mechanical planarization," *Proceedings of Electrochemical Society Meeting*, Vol. 96, pp. 228.

Bare, J.P., (2000). "Facilitization," In Li, S.H. and Miller, R.O. (Editors), *Chemical mechanical polishing in silicon processing, Semiconductors and Semimetals*, Vol. 63, Academic Press, San Diego, CA, pp. 47-87.

Bastawros, A.-F, Chandra, A., Guo Y., Yan, B., (2002), "Pad effects on material-removal rate in chemical-mechanical planarization," *Journal of Electronic Materials*, Vol. 31, no. 10, pp. 1022-1031.

Borucki, L., (2002), "Mathematical modeling of polish-rate decay in chemical-mechanical polishing," *Journal of Engineering Mathematics*, Vol. 43, pp. 105-114.

Brown, N.J., Baker, P.C., Maney, R.T., (1981), "Optical polishing of metals," *Proceedings of SPIE*, Vol. 306, pp. 42-57.

Chekina, O.G., Meer, L.M., Liang, H., (1998), "Wear-contact problems and modeling of chemical mechanical polishing," *Journal of the Electrochemical Society*, Vol. 145, no. 6, pp. 2100-2106.

Choi, J., Tripathi, S., Hansen, D., Dornfeld, D.A. (2006), "Chip scale prediction of nitride erosion in high selective STI CMP," *2006 CMP-MIC Conference*, pp. 160-167.

Fu, G., Chandra, A., Guha, S., Subhash, G., (2001), "A plasticity-based model of material removal in chemical-mechanical polishing (CMP), *IEEE Transaction on Semiconductor Manufacturing*, Vol. 14, pp. 406-417.

Fu, G., Chandra, A. (2001), "A model for wafer scale variation of removal rate in chemical mechanical polishing based on elastic pad deformation," *Journal of Electronic Materials*, Vol. 30, pp. 400-408.

Fu, G. (2002), "Modeling of chemical mechanical polishing at multiple scales," Ph.D. thesis, ISU.

Fu, G., Chandra, A., (2003), "An analytical dishing and step height Reduction Model for Chemical Mechanical Planarization," *IEEE Transactions on Semiconductor Manufacturing*, Vol. 16, no. 3, pp. 477-485.

Greenwood, J.A., Williamson, J.B.P., (1966), "Contact of Nominally Flat Surfaces," *Proceedings of the Royal Society of London*, A295, pp. 300-319.

Guo, Y., Chandra, A., Bastawros, A.-F., (2004), "Analytical Dishing and Step Height Reduction Model for Chemical Mechanical Planarization (CMP) with a Viscoelastic Pad," *Journal of Electrochemical Society*, Vol. 151, no. 9, pp. G583-G589.

Jaeger, R.C., (2002), "Introduction to microelectronic fabrication," Second edition, Prentice-Hall, New Jersey.

Jeong, S.-Y., Kim, S.Y., Seo, Y.J., (2003), "A study on the reproducibility of HSS STI–CMP process for ULSI applications," *Microelectronic Engineering*, Vol. 66, pp. 480-487.

Johnson, K.L., (1985), "Contact mechanics," CUP, Cambridge, New York.

Johnson, N.L., Kotz, S., (1970), "Distributions in Statistics: Continuous Univariate Distributions," Vol. 1, Wiley, New York.

Larsen-Basse, J., Liang, H., (1999), "Probable role of abrasion in chemo-mechanical polishing of tungsten," *Wear*, Vol. 233-235, pp. 647-654.

Laursen, T., Grief, M. (2002), "Characterization and optimization of copper chemical mechanical planarization," *Journal Electronic Material*, Vol. 31, no. 10, pp. 1059-1065.

Lee, W. S., Kim, S.Y., Seo, Y.J., Lee, J.K., (2001), "An optimization of tungsten plug chemical mechanical polishing (CMP) using different consumables," *Journal of Materials Science: Materials in Electronics*, Vol. 12 no. 1, pp. 63-68.

Li, S.H., Tredinnick, B., and Hoffman, M. (2000), "Consumables I: slurry". In LI, S.H. and

Miller, R.O.(Editors), *Chemical Mechanical Polishing in Silicon Processing, Semiconductors and Semimetals*, Vol. 63, Academic Press, San Diego, CA, pp. 139-153.

Luo, J., Dornfeld, D.A., (2001), "Material removal mechanism in chemical mechanical polishing: theory and modeling," *IEEE Transactions on Semiconductor Manufacturing*, Vol. 14, no. 2, pp. 112-133.

Luo, J., Dornfeld, D.A., (2003), "Effects of abrasive size distribution in chemical mechanical planarization: modeling and verification," *IEEE Transactions on Semiconductor Manufacturing*, Vol. 16, no. 3, pp. 469-476.

Luo, J., Dornfeld, D.A., (2004), "Integrated modeling of chemical mechanical planarization for sub-micron IC fabrication," Springer, Berlin Heidelberg, Germany.

Nanz, G., Camilletti, L., (1995), "Modeling of chemical mechanical polishing: A review," *IEEE Transaction Semiconductor Manufacturing*, Vol. 8, no. 4, pp. 382-389.

Oliver, M.R.(Editor), (2004), "Chemical mechanical planarization of semiconductor materials," Springer, New York.

Ouma, O. (1998), "Modeling of chemical mechanical polishing for dielectric planarization," Ph.D. thesis, MIT.

Ouma, O., Boning, D.S., Easter, W.G., Saxena, V., (2002), "Characterization and modeling of oxide chemical–mechanical polishing using planarization length and pattern density concepts," *IEEE Transactions on Semiconductor Manufacturing*, Vol. 15, no. 2, pp. 232-244.

Patrick, W.J., Guthrie, W.L., Standley, C.L., Schiable, P.M., (1991), "Application of chemical mechanical polishing to the fabrication of VLSI circuit interconnection," *Journal of the Electrochemical Society*, Vol. 138, no. 6, pp. 1778-1784.

Preston, F.W., (1927), "The theory and design of plate glass polishing machines" *Journal of Society Glass Technology*, Vo. 11, pp. 214-256.

Runnels, S. R., Renteln, P., (1993), "Modeling the effects of polish pad deformation on wafer surface stress distributions during chemical-mechanical polishing," *Dielectric Sciences Technology*, pp. 110-121.

Runnels, S. R., Eyman L.M., 1994, "Tribology analysis of chemical mechanical polishing," *Journal of the Electrochemical Society*, Vol. 141, no. 6, pp. 1698-1701.

Shan, L., (2000), "Mechanical interactions at the interface of chemical mechanical polishing," Ph.D. thesis, GIT.

Shi, F.G., Zhao, B., Wang, S.Q., (1998), "A new theory for CMP with soft pads," *Proceedings of International Interconnect Technology Conference*, San Francisco, CA, pp. 73-75.

Singer, P., (1998), "Tantalum, copper and damascene: The future of interconnects," *Semiconductor International*, Vol. 21, no. 6, pp. 90-98.

Sivaram, S., Bath, H., Lee, E., Leggett, R. and Tolles, R., (1992), "Measurement and modeling of pattern sensitivity during chemical-mechanical polishing of interlevel dielectrics," *SEMATECH*, Technical Report, Austin, TX.

Smith, T.H., Fang, S.J., Boing, D.S., Shinn, G.B., Stefani, J.A., (1999), "A CMP model combing density and time dependencies," *2005 CMP-MIC Conference*, pp. 97-104.

Stavreva, Z., Zeidler, D., Plotner, M., Drescher, K., (1997), "Influence of process parameters on chemical-mechanical polishing of copper," *Microelectronic Engineering*, Vol. 37-38, pp. 143-149.

Stein, D., Hetherington, D., Dugger, M., Stout, T., (1996), "Optical interferometry for surface measurement of CMP pads," *Journal of Electronic Materials*, Vol. 25, pp. 1623-1627.

Steigerwald, J.M., Murarka, S.P., Gutmann, R.J., (1997), "Chemical mechanical planarization of microelectronic materials," *John Wiley & Sons Pub.*, New York.

Stine, B., Mehrotra, V., Boning, D., Chung, J., Ciplickas, D., (1997), "A Simulation Methodology for Assessing the Impact of Spatial/Pattern Dependent Interconnect Parameter Variation on Circuit Performance," *IEDM Tech, Digest*, pp. 133-136.

Sundararajian, S.,Thakuta, D.G. Schwendeman D.W.,Murarka, S.P., Gill, W.N., (1999), "Two-dimensional wafer-scale chemical mechanical planarization models based on lubrication theory and mass transport," *Journal of the Electrochemical Society*, Vol. 146, no. 2, pp. 761-766

Thakurta, D.G., Borst, C.L., Schwendeman, D.W., Gutmann, R.J., Gill, W.N., (2000), "Pad porosity, compressibility and slurry delivery effects in chemical-mechanical planarization: modeling and experiments," *Thin Solid Films*, Vol. 366, no. 1-2, pp. 181-190.

Thakurta, D.G., Schwendeman, D.W., Gutmann, R.J.,Shankar, S., Jiang, L., Gill,W.N., (2002), "Three-dimensional wafer-scale copper chemical-mechanical planarization model," *Thin Solid Films*, Vol. 414, no. 1, pp. 78-90.

Tichy, J., Levert, J.A., Shan, L., Danyluk, S., (1999), "Contact mechanics and lubrication hydrodynamics of chemical mechanical polishing," *Journal of the Electrochemical Society*, Vol. 146, no. 4, pp. 1523-1528.

Vlassak, J.J., (2004), "A model for chemical–mechanical polishing of a material surface based on contact mechanics," *Journal of the Mechanics and Physics of Solids*, Vol. 52, pp. 847-873.

Wang, C., Sherman, P.J., Chandra, A., (2005), "A stochastic model for the effects of pad surface topography evolution on material removal rate decay in chemical-mechanical planarization," *IEEE Transactions on Semiconductor Manufacturing*, Vol. 18, no. 4, pp 695-708.

Wang, C., Sherman, P.J., Chandra, A., Dornfeld, D., (2005), "Pad surface roughness and slurry particle size distribution effects on material removal rate in chemical mechanical planarization" *CIRP Annals - Manufacturing Technology*, Vol. 54, no. 1, pp. 309-312.

Warnock, J., (1991), "A two-dimensional process model for chemical mechanical polish planarization," *Journal of the Electrochemical Society*, Vol. 138, no. 8, pp. 2398-2402.

Wolf, S., (1990), "Silicon Processing for the VLSI Era: Vol. 2 - Process Integration," Lattice Press, Sunset Beach, CA, Chapter 4.

Xie, X., Boning, D.S., Meyer F., Rzehak, R. and Wagner, P. (2006), "Analysis and modeling of nanotopography impact in blanket and patterned silicon wafer polishing," *2006 CMP-MIC Conference*, pp. 243-253.

Yu, T.K., Yu, C.C., Orlowski, M., (1993), "A statistical polishing pad model for chemical–mechanical polishing," *Proceedings of the IEEE International Electron Devices Meeting*, pp. 35.4.1- 4.

Zeng, T., Sun, T., (2005), "Size effect of nanoparticles in Chemical mechanical polishing-A transient model", *IEEE Transactions on Semiconductor Manufacturing*, Vol. 18, no. 4, pp. 655-663.

Zhao, B., Shi, F. G., (1999), "Chemical mechanical polishing in IC process: New fundamental insights," *Proceeding of Fourth International Chemical-Mechanical Planarization for ULSI Multilevel Interconnection Conference*, Santa Clara, CA, pp.13-22.

Zhao, Y., Chang, L., (2002), "A micro-contact and wear model for chemical-mechanical polishing of silicon wafers," *Wear*, Vol. 252, pp. 220-226.